Department of Physics and Astronomy
Ruprecht-Karls-Universität Heidelberg

bachelor thesis in physics
submitted by

Dominick Cichon

born in Mannheim (Germany)

2013

Examining Hamamatsu R11410-21 photomultipliers for XENON1T at room and liquid xenon temperatures

This bachelor thesis has been carried out by Dominick Cichon at the
Max-Planck-Institut für Kernphysik in Heidelberg
under the supervision of
Prof. Dr. Manfred Lindner

Abstract:
Photomultipliers (PMTs) play a critical role in detecting liquid xenon scintillation light for the planned XENON1T experiment, while also having to meet high standards, especially regarding quantum efficiency and intrinsic radioactivity levels. To meet those standards, the R11410-21 PMT series has been developed by Hamamatsu Photonics in cooperation with the XENON collaboration. During the course of this bachelor thesis, various tests of PMTs of this series have been made at the Max-Planck-Institut für Kernphysik, Heidelberg, in order to determine parameters relevant for the experiment, like gain, dark count rate, transit time spread and afterpulse-to-main-pulse ratio and to verify specifications given by the producer. Because the PMTs will operate in XENON1T at approximately −100 ℃, a specifically designed cool down setup has been used along with a room temperature setup, which has previously been used to test PMTs for the Double Chooz experiment. This allowed testing at room temperature as well as at cryogenic temperatures. Results have verified most of the values given by Hamamatsu and give a positive outlook for usage of the PMT series in XENON1T.

Zusammenfassung:
Photomultiplier (PMTs) spielen eine wichtige Rolle beim Detektieren von Szintillationslicht von flüssigem Xenon für das geplante XENON1T-Experiment, wobei sie zugleich hohen Ansprüchen, insbesondere in Sachen Quanteneffizienz und intrinsische Radioaktivität, genügen müssen. Um dies zu bewerkstelligen, entwickelte Hamamatsu Photonics in Kooperation mit der XENON-Kollaboration die R11410-21-PMT-Reihe. Im Laufe dieser Bachelorarbeit wurden verschiedene Tests am Max-Planck-Institut für Kernphysik in Heidelberg durchgeführt, um Parameter wie die Verstärkung, die Dunkelrate, die Transitzeitverbreiterung sowie das Verhältnis Nachpulse zu Hauptpulse zu bestimmen und um die Angaben des Herstellers zu verifizieren. Da die PMTs in XENON1T bei etwa −100 ℃ betrieben werden, wurde neben einem Raumtemperatur-Messaufbau, der zuvor benutzt wurde, um PMTs für das Double-Chooz-Experiment zu testen, ein spezieller Kühlaufbau verwendet. Dies machte es möglich, sowohl bei Raumtemperatur, als auch bei tiefen Temperaturen zu testen. Die aus den Tests gewonennen Resultate haben einen Großteil der Herstellerangaben bestätigt und liefern positive Aussichten bezüglich der Verwendung der PMT-Reihe für XENON1T.

Contents

1. Introduction and theory

During the course of this bachelor thesis, several R11410-21 photomultipliers (PMTs) supplied by Hamamatsu Photonics [Ham] were tested at different temperatures for usage in the future XENON1T experiment [Apr12]. After a short introduction to the topic of dark matter and its possible detection with the aforementioned experiment, the working principle of a PMT and its main characteristics are outlined.

1.1. Dark matter and XENON1T

1.1.1. The search for dark matter

Several observations, reaching back to the beginning of the 20th century, have shown, that visible matter seems to make up only a small percentage of the entire matter in the universe. Because the remaining matter does not interact via electromagnetic or strong force, as otherwise it would have already been detected, it is called "dark matter". One of the most promising candidates today is a hypothetical **w**eakly **i**nteracting **m**assive **p**article (WIMP) [Sch08], which only interacts via gravitational and weak forces. Thus, experiments hoping to find it require very low background rates respectively very good dark-matter-signal-to-background discrimination as well as large target masses.

In general, there are three possible ways to detect a WIMP if it exists [Ber10].

- One way would be creating it in a particle accelerator like the Large Hadron Collider at CERN [LHC], looking for collision events with missing energy.
- Another way would be indirect detection by measuring products of dark matter annihilation. As WIMPS accumulate within certain astronomical regions, those products can be detected by using telescopes suited for this task.

- Lastly, direct detection aims to measure the energy a WIMP deposits into a target material when it scatters elastically with the target's nuclei.

1.1.2. The XENON1T experiment

A series of such direct detection experiments is the XENON Dark Matter Project, where two experiments already have taken data (XENON10 [Apr+11] and most recently XENON100 [Apr+12]), while a third experiment, XENON1T [Apr12], has gone into construction phase. Each of them consists of a liquid xenon time projection chamber (TPC), shielded from background radiation by different materials and by being located underground at the Laboratori Nazionali del Gran Sasso [LNGS] in Italy. Each subsequent experiment roughly uses 10 times more liquid xenon and has a 100 times lower background than the previous one. XENON1T is, as the name may imply it, going to use around 1 t of liquid xenon as a fiducial volume for detection, scintillating if particles deposit energy on it. Photons (S1 signal) as well as charge (free electrons) are produced by interactions with xenon, the latter drifting into the upper part of the tank due to a homogenous electromagnetic field being created by metallic meshes. There, xenon is in its gas phase, and the free electrons cause a cascade of particles in the upper part by being accelerated further and hitting xenon atoms. This results in an amplification of the signal and a proportional amount of photons being created (S2 signal). All the xenon as well as all of the aforementioned equipment are to be housed within a cryostat suspended into a larger tank filled with ultrapure water, which acts as a shield and as a muon veto.

Events are to be detected by two photomultiplier (PMT) arrays: One on the bottom of the TPC, submerged in liquid xenon, and one at the top in the gas phase. Both arrays detect S1 and S2 signals, allowing one to determine at which height of the tank an event happened by looking at the time differences between both signals. As the XENON collaboration aims to get sensitivities for WIMP cross-sections as low as $\sigma \approx 2 \times 10^{-47}\,\mathrm{cm}^2$ for certain possible WIMP masses, it requires extremely low background for its experiments. Consequently, the PMTs need to be made out of materials with very low intrinsic radioactivity, causing only few mBq/PMT. Furthermore, they need to have high detection efficiencies in order to gain enough statistics per event to determine particle energy with reasonable accuracy.

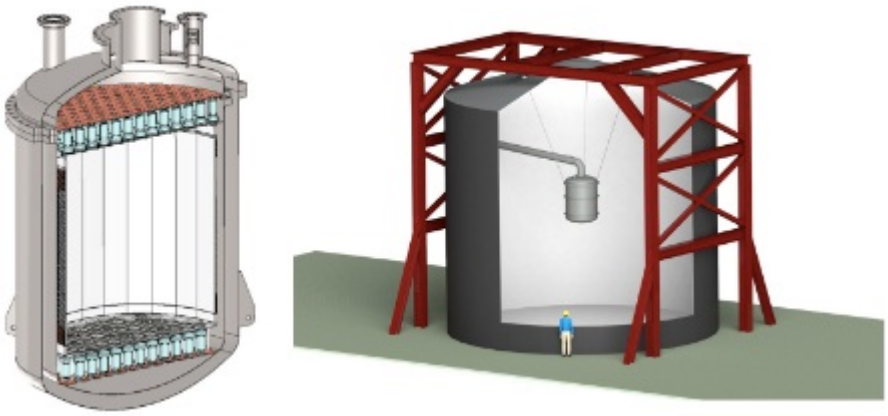

Figure 1.1.: Cross section of the planned XENON1T experiment. The left side shows the TPC, while the right side shows the cryostat. (taken from [Apr12])

1.2. Photomultipliers (PMTs)

To choose PMTs suited for an experiment like XENON1T, it is essential to know how they actually work and which of their parameters are relevant for the experiment [Ham07]. In the following section, an overview of how a PMT works and some of its related parameters is made.

1.2.1. Working principle of a PMT

As shown in figure 1.2, an incoming photon hits the PMT's photocathode, which consists of a special coating reactive to light. There, it is absorbed with a certain probability and causes an electron to be emitted, if the photon's energy was high enough, utilizing the external photoelectric effect. Such an electron is called a “photoelectron”. Entering the interior of the PMT, which is in vacuum to avoid the photoelectron colliding prematurely with gas atoms/molecules, it is accelerated towards the first dynode, which is at a more positive voltage than the cathode, via an electric field. Acceleration is assisted by a focusing electrode. After hitting the first dynode, several electrons are emitted from it, multiplying the amount of electrons. All those electrons are accelerated towards the second dynode, which is at a more positive voltage than the first one. This procedure is repeated with additional dynodes, creating a growing cascade of electrons, until the last one is hit. After that, the electrons are not accelerated towards another dynode, but to the PMT's anode. There, they are collected and cause a

measurable electric current, which, in general, is directly proportional to the amount of electrons initially being emitted from the photocathode.

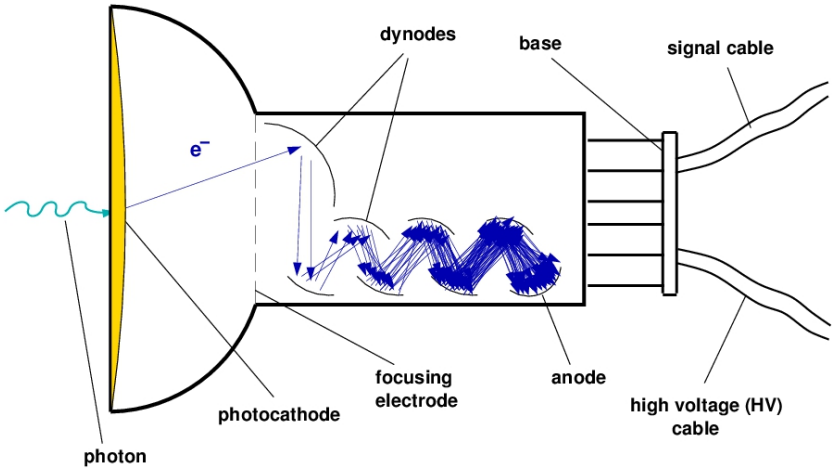

Figure 1.2.: PMT working principle schematic

Because the initial signal is amplified strongly by this design, PMTs are capable of single photon detection, essential for measuring rare events, especially those which only cause very few photons to be emitted. To ensure this capability as well as generally good detection performance, it is necessary to choose an optimum dynode layout as well as appropriate voltages for them. For the latter task, the electronic components of the voltage divider, also called “base”, which divides the voltage applied to the PMT among the dynodes, have to be chosen correspondingly.

1.2.2. Important parameters and phenomena

For using a PMT in an experiment, it is vital to know important parameters and phenomena associated with it for data analysis. Both are outlined in the following section:

- **Quantum/collection efficiency:**
  A PMT's total detection efficiency is made up by two factors. One of them, the quantum efficiency, is the probability of a photon hitting the photocathode to produce a photoelectron, while the other one, the collection efficiency, gives the probability of a produced photoelectron hitting the first dynode. The total efficiency, calculated by multiplying those factors, is of great importance, as mea-

suring more of the incoming photons means getting more statistics in a shorter amount of time, and, more importantly, a better energy resolution per event.

- **Linearity and voltage divider design:**
  Because large electron currents cause changes in the voltage between two dynodes, saturation effects begin to appear after a certain amount of photons detected. Thus, it is important to know up to which number of incident photons a PMT's response is linear, which is a prerequisite for reliable calculations, especially those involving the gain factor outlined below. To improve linearity, the components of the voltage divider plugged onto a PMT can be chosen correspondingly. Usually, several base designs have to be tested to find one with the desired linearity characteristics.

- **Gain:**
  The gain factor g is the factor by which a single photoelectron is amplified via dynode multiplication. It is given by the ratio of the charge Q_{SPE} flowing through the PMT's anode when a single photon has been detected and the elementary charge e:
  $$g = \frac{Q_{SPE}}{e}. \tag{1.1}$$
  One needs to know this factor to determine the amount of photons which have caused a single pulse, given that the PMT behaves linearly. As it is often the case in experiments that the amount of photons emitted is proportional to the total amount of energy emitted by the photon source (for example a scintillator), it also allows determining the energy of a measured event. Furthermore, a high intrinsic gain is desirable, because it means that less additional signal amplification via electronics, which could introduce additional noise, is needed. Also, a higher gain allows to better separate charge created by photoelectrons from charge caused by noise pulses. This is important for discerning single photoelectron (SPE) events from noise, by allowing the trigger electronics, which are usually used for this task, to trigger at lower pulse heights. In turn, this leads to a higher detection efficiency as well as a better energy resolution. Two related resolution parameters, the “SPE peak resolution” and the “peak-to-valley ratio”, are outlined in section 3.1.1.

- **Dark count rate:**
  Even without a photon source, free electrons are emitted inside a PMT, mainly via thermal emission, but also via ionization and radioactive emission. Those are detected and multiplied as real photoelectrons are, leading to so called dark pulses, indistinguishable from real ones in terms of pulse topology. Although by far most events caused by such pulses can be discarded via appropriate coincidence criteria, random coincidences may still appear, meaning that the dark count rate needs to be kept low to minimize their probability.

- **Transit time spread:**
  Because different points on the photocathode have a different distance to the first dynode and the electric field inside the PMT is not homogenous, the time between the absorption of a photon and the resulting pulse is not sharply defined, but "smeared", with the transit time following a certain distribution. For determining coincidences with a high temporal resolution, it is vital for this distribution to have a small width, i.e. a small "transit time spread".

- **Early pulses:**
  Early pulses happen, when a photon goes through the photocathode and creates an electron at one of the dynodes, typically the first one. As photons are naturally faster than the photoelectrons produced, a pulse is registered earlier than usual. Because at least one step of the dynode multiplication process is skipped, those pulses contain less charge in general.

- **Late pulses:**
  Late pulses are pulses occurring a few nanoseconds after a regular pulse, being caused by electrons being scattered at the first dynode and not multiplied by it. Those electrons then, accelerated by the electric field, hit the dynode again, usually being multiplied regularly this time. This results in a late pulse, as the scattered electrons are slightly delayed relative to the electron cascade, which also means that a portion of the total charge of the main pulse is delayed as well. For determining a pulse's charge, this has to be considered by integrating over both main and late pulses. Otherwise, part of the charge would get lost, resulting in systematic errors.

- **Afterpulses:**
  Due to its materials emanating gas, the interior of a PMT is not perfectly vacuumized. Instead, slight amounts of gas accumulate. Photoelectrons, given

enough energy, are able to collide with this gas and create positively charged ions, which drift towards the photocathode because of the electric field. There, they are able to release one or more electrons, which behave exactly like regular photoelectrons and cause a pulse, called “afterpulse”. These pulses usually appear several 100 ns or later after a main pulse. For the same reasons as with the dark rate, the number of afterpulses should be as low as possible to avoid random coincidences. On the other hand, looking at the temporal afterpulse distribution allows one to identify several gases present in the PMT, if the arrival time for identical masses is roughly the same, as molecules with different masses are differently accelerated. This results in different travel times, making the PMT usable as a crude mass spectrometer. For the PMTs tested, the aforementioned criterion was met, as confirmed at the University of California and Hamamatsu [Lun+12]. The reason for it seems to be the structure of the electric field inside the PMT, indicated by simulations done by the University of Zürich [Bar].

- **Intrinsic radioactivity:**
  For usage in experiments needing a very low background, the materials the PMT is made of are not allowed to be too radioactive. Especially in cases like XENON1T, where the constraints to radioactivity are extreme because of the detector's targeted sensitivity, those materials need to be screened and selected carefully while, at the same time, other operative parameters have to kept as good as needed.

- **Thermal robustness:**
  As the PMTs need to operate at about −100 ℃ in the case of XENON1T, it is imperative for them to withstand thermal stress and to be capable to operate at such temperatures. Also, their characteristics should be stable at constant temperature while not worsening at the same time.

1.3. PMT-testing

XENON1T needs PMTs with the highest possible quantum efficiencies as well as extremely low radioactivity to lower the detection threshold. Hamamatsu Photonics, in cooperation with the XENON collaboration, has developed the R11410 series, which

aims to meet those high requirements. Its main features are very high quantum efficiencies (up to 41 % have already been reached) and extremely low intrinsic radioactivity.

Up to now, three versions were available, released in the following order: MOD, 10 and 21. Differences between them are only very minor, with one of them being a change of an aluminum seal between 10 and 21, the goal being reducing radioactivity even further. The latter is scheduled to be the version used in XENON1T.

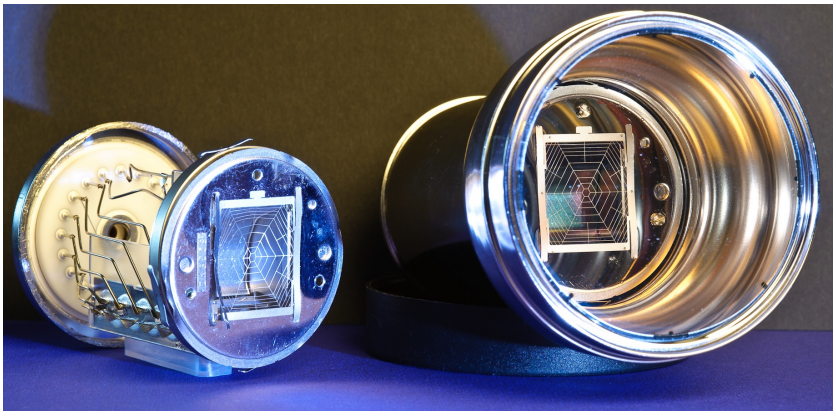

Figure 1.3.: Two R11410 PMTs, the left one having its window and body removed.

Although Hamamatsu is testing each PMT themselves before it is sent to the XENON collaboration, there still is a need for several tests by the collaboration itself. One of the reasons is to verify Hamamatsu's results, ensuring that the PMTs sustained no damage during transportation, as it is critical that they work as desired before being mounted into XENON1T. Another reason is to better understand PMT behavior and possible parameter correlations, especially at conditions similar to those it will face in the experiment, which means that cold temperature tests at about −100 ℃ have to be made. This should prove very useful to determine potential error sources stemming from PMTs being used as well as for correcting respectively avoiding them.

Thus, several important parameters, as outlined in chapter 3, are measured for a number of R11410-21 PMTs, with some PMTs of previous versions also being used in a number of measurements, as they should perform similarly. Those results are then compared to the specifications given by Hamamatsu, some of which are outlined in the following section.

1.3.1. Typical parameter values for a R11410-21 PMT given by Hamamatsu

Important typical values given by Hamamatsu [Ham] for the 21 version are as follows:

- A **quantum efficiency** of 32.5 % at $\lambda = 175\,\mathrm{nm}$, which is the wavelength at which liquid xenon scintillates.
- A guaranteed **upper radioactivity limit** of 5 mBq for Th and U chains, 20 mBq for the ^{40}K chain, 5 mBq for the ^{60}Co chain and 50 mBq for the ^{137}Cs chain.
- A **gain** of 5×10^6 at 1500 V.
- **Dark count rates** of 4000 Hz at 25 ℃ and 50 Hz at −100 ℃.
- A **transit time spread** of 9 ns.
- An **afterpulse-to-main-pulse ratio** within the first two microseconds after a main pulse of maximally 10 %.

According to specifications by Hamamatsu, the quantum efficiency for the first 60 PMTs delivered is, on average, around 37.5 %. Also, the XENON collaboration has measured average PMT radioactivity levels for the aforementioned chains to be $<$ 1 mBq for Th and U, $\approx$ 12 mBq for ^{40}K and $\approx$ 1 mBq for ^{60}Co [XEN]. Average values for gain, dark count rate, TTS and afterpulse-to-main-pulse ratio are determined in chapter 3.

2. Experimental setup

For testing the performance of the R11410 PMTs, two different experimental setups were used, both being light-tight and sharing the same electronics for PMT data acquisition: A testing array situated inside a Faraday cage for measuring at room temperature, and a Dewar vessel surrounded by a metal casing for measuring at low temperatures (down to −110 ℃). The latter requires additional equipment for monitoring temperature and pressure. Both setups are located at the Max-Planck-Institut für Kernphysik (MPIK) in Heidelberg, Germany. Because the voltage divider used during measurement affects parameters of the PMT it is mounted on, its design will also be illustrated.

2.1. Room temperature setup

Originally constructed to analyze PMTs for the Double Chooz experiment [Bau+11; Has10; Luc09; Kae], the PMT array provides an ideal environment for testing at room temperature, allowing, in principle, up to 30 PMTs to be examined simultaneously. It is located within a Faraday cage in order to suppress noise, which also acts as a darkroom.

The cage itself, internally covered with black cloth to reduce reflections and kept dark during measurement, provides shielding against light as well as electronic noise and houses an array of 30 PMT slots, with an optical fiber mounted in front of each slot, which is connected to a blue LED ($\lambda = 380\,\mathrm{nm}$) (see figure 2.1). Each slot receives light from a different LED, allowing to illuminate each PMT individually with different timing settings and intensities. For testing the XENON1T candidate PMTs, 12 slots were used. As regards temperature, the cage is in thermal equilibrium with the room it is located in. Because the latter is air-conditioned, room temperature is very stable,

varying less than 0.5 ℃ over an entire day (barring extreme weather changes), with its mean around 20 ℃ to 25 ℃.

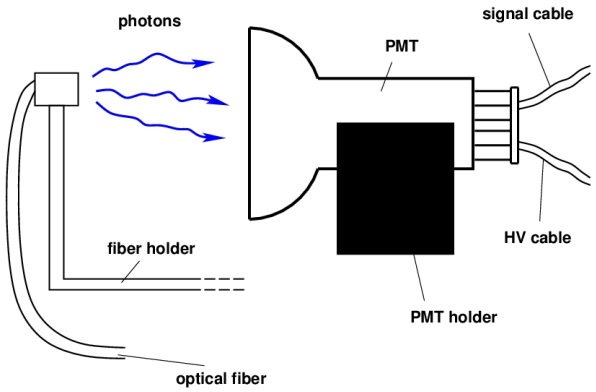

Figure 2.1.: Side view of an array slot (schematic).

To supply the PMTs with high voltage as well as to pass on their signals, their cables are connected to respective extensions which are led outside of the cage via light-tight feed-throughs. In total, a cable length of $\approx 19\,\mathrm{m}$ is reached.

2.2. Cooling setup

As a liquid xenon system capable of testing at least 10 PMTs or more would require major efforts and much longer cooldown times, an alternative had to be found. Specifically for this task, a simpler cooling system was designed, which uses liquid nitrogen and is capable of holding up to 12 PMTs to be measured.

The PMTs are mounted on two almost identical structures (figure 2.2), which contain holders for Pt100 sensors, as well as for, in total, 3 optical fibers, used for uniformly illuminating all PMTs for several measurements. Furthermore, the PMTs are arranged in such a way, that each of them faces another.

The structures are lowered into a large Dewar vessel, which itself is surrounded by a metal tank (figure 2.2). Welded to the inward facing side of the casing's lid, a copper coil is used for cooling by letting liquid nitrogen (LN) flow through it. The lid also contains an input/output for gaseous nitrogen (GN), a manometer and a mounting point for an additional pressure sensor. Furthermore, it has openings to avoid too high pressure as well as feed-throughs where potting is used. Through them, extensions for

the PMTs' signal and HV cables as well as for the optical fibers are led, leading to a total cable length of about 10 m for the first two. After everything is in place, the lid is screwed onto the tank and tests are made to ensure that the tank is light-tight.

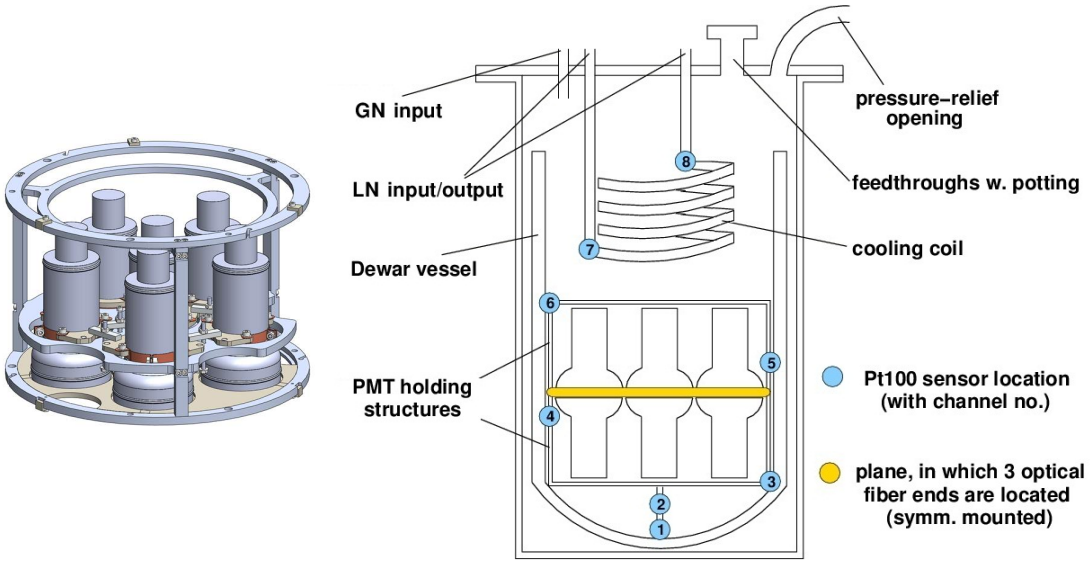

Figure 2.2.: (Left) Schematic of PMT holding structure. (Right) Schematic of cooling setup.

Great care hast to be taken while changing the setup's temperature, as the PMTs, according to Hamamatsu's specifications, must not change temperature faster than $2\,\mathrm{K/min}$. Also, temperature needs to be kept stable within $\pm\,4\,\mathrm{K}$ for approximately $3\,\mathrm{h}$ to ensure that all measurements can be made. Possible gradients near the location of the PMTs had to be minimized, with a maximum temperature difference of 15 ℃ between structure ends being encountered during cooldowns. Because PMTs mainly consist of metals, gradients within it can be assumed to be lower because of better thermal conductivity. To provide enough thermal isolation in order to minimize warmth intake as well as to slow down the warm up process, aluminum tape has been sticked onto both sides of the lid as well as the upper part of the metal casing. Additionally, the latter has also been covered with polystyrene foam on the outside. These measures, along with the isolation provided by the Dewar vessel, are sufficient to keep change rates below the specified limit during warm up.

For finding an optimum procedure for cooling down and warming up the tank, several test runs had to be made. For the first several minutes, the tank is flushed with GN in order to to displace air inside it and thus eliminating possible water condensa-

tion, as it would otherwise potentially cause harm to the PMTs mounted. Then, after flushing has stopped, LN passes through the cooling coil with such a flow, that the zone in which the PMTs are located is cooled down very slowly (around 0.5 K/min) until the target temperature (−100 °C) has been reached. Following that, the flow of LN is carefully varied to keep temperature stable (keeping fluctuations below ±2 ℃ is possible with the setup) and to minimize temperature gradients. Warming up is done by simply stopping nitrogen flow, as the tank's isolation has proven to be enough to keep changing rates well below the value specified by Hamamatsu, taking more than a day to reach room temperature again.

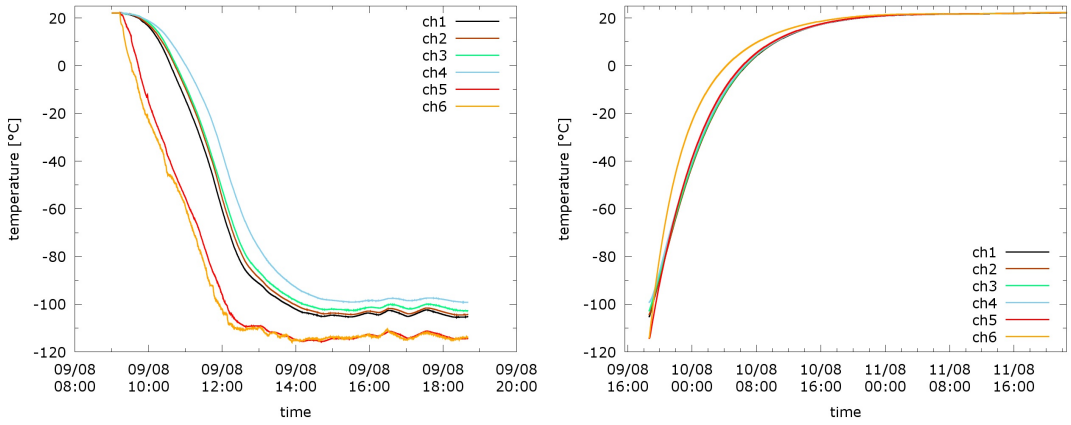

Figure 2.3.: Temperature profile of a cooldown. For the cooldown depicted, a temperature of −113 ℃/−99 ℃ for the upper/lower holding structure (taking the average of both of its thermal sensors) was held for about three hours, with a standard deviation of 1 ℃/2 ℃. (Left) Cooling down. (Right) Warming up.

Figure 2.3 shows the temperatures measured by the different Pt100 sensors during a cooldown, with the channels shown being ordered according to the respective sensor's height in the setup, channel 1 being the lowest (as shown in figure 2.2). As channel 6 is the closest to the cooling coil of the channels shown, it is also the most sensitive to changes in nitrogen flow, resulting in higher change rates and a higher temperature difference to the other sensors being measured, also visible in the diagram. One would probably expect that channels located at a lower height would have, at first, higher temperatures than those at a higher height, because the latter are closer to the cooling coil. With the PMT holding structure blocking respectively altering circulation and changing warmth flow, however, a channel's height does not necessarily correspond to its temperature.

2.3. PMT voltage divider

The voltage divider (base) layout (circuit diagram in figure A.1) for the XENON1T experiment has been designed by the University of Zürich, aiming at optimum linearity even for large pulses. At the same time, heat dissipation had to be minimized.

Figure 2.4 shows all sides of the base. On both of them, conducting paths as well as resistors (black) are visible, while on the upper side, capacitors (gray) can also be seen. The resistors are chosen such, that they comply to a certain ratio recommended by Hamamatsu (table 2.1), which, according to them, ensures optimum dynode voltage division. To get the resistor values needed, they have to be multiplied by $R_b = 5\,\mathrm{M\Omega}$, which has been chosen as the base resistor value. 5 capacitors with a capacity of 10 nF each, located between the last five dynodes, provide additional charge to guarantee linearity at large pulses, i.e. large electron currents.

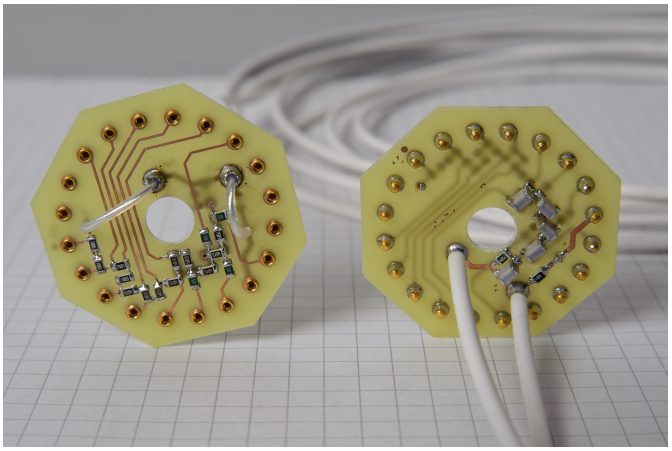

Figure 2.4.: Photo of the base used.

resistor	R_k	R_1	R_2	R_3	R_4	R_5	R_6	R_7	R_8	R_9	R_{10}	R_{11}	R_a
value [R_b]	4	1.5	2	1	1	1	1	1	1	1	1	1.5	1.5

Table 2.1.: Resistor ratios as recommended by Hamamatsu
R_k: between cathode and 1st dynode - R_i: between ith and $i+1$th dynode - R_a: between 12th dynode and anode

2.4. Electronics and monitoring system

In the following, the electronics used for signal processing and data acquisition as well as the cooling setup's monitoring system are described.

2.4.1. PMT data acquisition system

Like the testing array mentioned in section 2.1, the PMT data acquisition system has been originally conceived to test PMTs for the Double Chooz experiment [Bau+11; Has10; Luc09; Kae]. As outlined in figure 2.5, each PMT's output signal is being fed through separate channels. There, they are sent through an amplifier (10x), then split amongst two different outputs by a fan out module.

One of those two outputs is connected to a second amplifier (also 10x), going to a discriminator, which sends a logical pulse if the incoming signal passes a certain, adjustable threshold. This logical pulse is then being sent to two different devices: To a scaler, capable of counting incoming logical signals for several inputs, and to a time-to-digital converter (TDC)l, which is capable of measuring the time which has passed between two signals. The maximum time difference which can be measured is 1.2 µs, with a resolution of $\Delta t = 0.3\,\mathrm{ns}$. The measured differences are used to construct a time histogram.

The other output directly leads to a charge-to-digital converter (QDC), which integrates over the incoming signal within a certain time interval ($\approx 200\,\mathrm{ns}$) determined via a trigger signal, with the signal's width being equal to the integration window. This allows to measure how much charge has flown through the respective PMT's anode and, by extension, how many photoelectrons have been emitted by the photocathode (once the PMT's gain factor is known). The QDC can measure charges up to 400 pC, with a resolution of $\Delta q = 0.0976\,\mathrm{pC}$. Analogous to the TDC measurements, the measured charges lead to a charge histogram.

TDC, scaler and QDC are fed to a computer, sending their data to it, which saves the corresponding parameters as well as the current Unix time. A trigger board, connected to the same computer and controlled by it, contains several outputs which can be adjusted to send trigger signals with a certain frequency. Trigger signals are used for specifying the QDC integration window, for providing a start signal for the TDC as

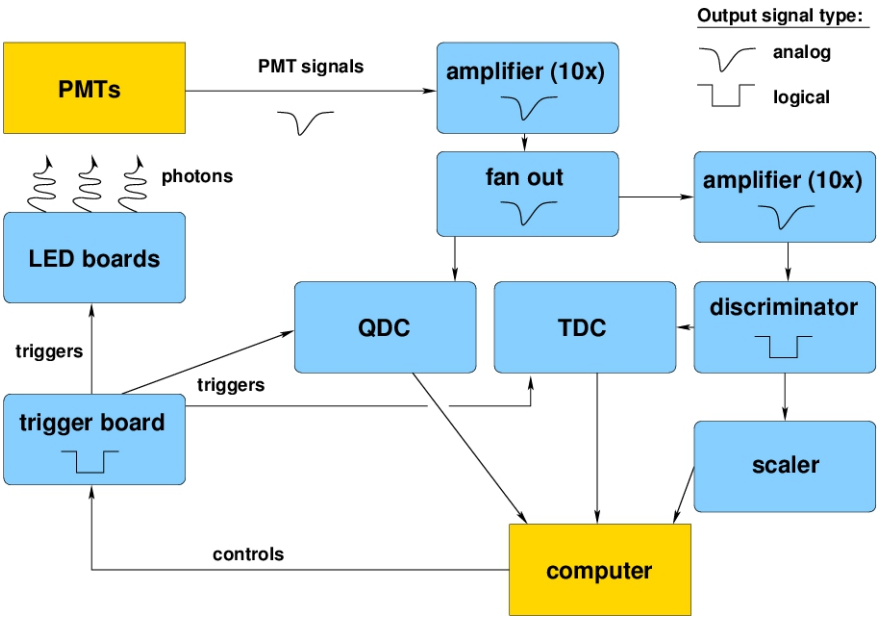

Figure 2.5.: Signal flowchart.

well as for activation of several LED boards at specified times. Those boards contain multiple LEDs mounted inside them, which are the ones the optical fibers mentioned in section 2.1 and section 2.2 are connected to and send photons when receiving a trigger signal. Each LED intensity can be adjusted separately.

Data processing is performed offline with the help of different self written C-programs, the results being written into a database file for each test run. A majority of those programs had already been written for Double Chooz PMT testing and could be reused. Details of the data analysis are outlined in chapter 3.

2.4.2. Pressure/temperature monitoring system

For temperature measurement during a cooldown of the cooling setup, a W&T 57607 web thermograph [WuT], capable of measuring with 8 different sensors at the same time, has been used with the same amount of three-wire Pt sensors. The sensors are located at different heights in the cooling setup in order to measure absolute temperature, its evolution in time as well as temperature gradients. The sensors had to be calibrated, because a large temperature offset was present, probably due to the length of the wires (3 m) causing a non-negligible conductor resistance. Calibration was done via measuring different reference temperatures and comparing the sensors' values T_i'

with those of an accurately calibrated four-wire sensor. Reference temperatures were taken from the current room temperature, liquid argon and liquid xenon as well as ethanol cooled with liquid nitrogen to several different temperatures. Every channel has shown to be linearly related to the real temperature T_i:

$$T_i = a\,T_i' + c \tag{2.1}$$

with a and b being determined by a linear fit. As an example for such a fit, the calibration curve of sensor channel 1 is shown in figure 2.7. The mean values of the fit parameters for all channels are $\overline{a} = 0.9862 \pm 0.0007$ and $\overline{c} = (-14.24 \pm 0.07)\,°\mathrm{C}$. a and c also vary only slightly between each channel, with $\sigma_a = 7 \times 10^{-4}$ and $\sigma_c = 0.08\,°\mathrm{C}$.

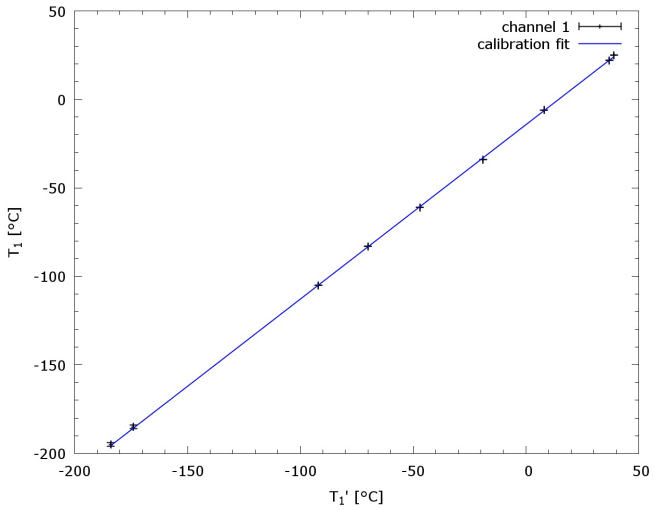

reference temperature	$T_1'[°C]$	$T_1[°C]$
room temperature	39.80 ± 0.05	25.3 ± 0.4
ethanol (uncooled)	37.43 ± 0.05	22.5 ± 0.4
ethanol (cooled) 1	8.33 ± 0.05	-6.2 ± 0.3
ethanol (cooled) 2	-19.94 ± 0.05	-34.1 ± 0.5
ethanol (cooled) 3	-47.55 ± 0.05	-61.1 ± 0.6
ethanol (cooled) 4	-70.42 ± 0.05	-83.8 ± 0.7
ethanol (cooled) 5	-92.24 ± 0.05	-105.2 ± 0.8
liquid argon	-174.40 ± 0.05	-185.9 ± 1.2
liquid nitrogen	-184.51 ± 0.05	-195.7 ± 1.3

Figure 2.7.: Calibration curve of channel 1. T_1' represents the temperature measured by the uncalibrated sensor, while T_1 is the value provided by the reference sensor.

Pressure inside the setup was measured via a Greisinger GMH3111 pressure sensor [Gre], with its sensing element mounted on top of the cooling setup's lid. It was measured relative to atmospheric pressure for safety reasons to indicate, if too much pressure has built up inside the tank. Apart from $\approx 6\,\mathrm{mbar}$ at most while flushing the Dewar vessel with liquid nitrogen, no overpressure was measured.

Both devices were connected to a PC running a LabVIEW program [NIC], which displays the data online and saves it for later analysis and correlations with PMT data. The program also provides several features like recording how often the measured temperature change rate passed a certain, customizable threshold during each measurement.

3. Measurements and results

In this chapter, all relevant PMT measurements will be outlined. Each section describes why a certain parameter is important, how it has been measured, how the data taken has been analyzed, how the results can be interpreted and how they compare to specifications given by the producer, Hamamatsu Photonics. With the available setups, measurements of a PMT's gain, dark count rate, transit time spread as well as its afterpulse-to-main-pulse ratio at room temperature were made. For the first two parameters, tests were alse made at approximately liquid xenon temperature. For the latter two, the transit time spread and the afterpulse-to-main-pulse ratio, no measurements at liquid xenon could be made, as illumination control of the cooling setup has not been sufficient enough to allow these measurements.

3.1. Gain

The gain describes the factor by which a single photoelectron is amplified by the dynode chain of a PMT. As it determines how well single photoelectron events can be detected and differentiated from noise events, it is crucial for reaching a certain resolution.

3.1.1. Measurement method and data analysis

For measuring gain, a charge histogram has to be taken using a QDC module, while illuminating the PMT at single photoelectron (SPE) intensity. A measurement time of typically 400 s has been chosen, which usually is sufficient to acquire enough statistics. If the mean charge for SPE events is known, one can divide it by the elementary charge [see equation (1.1)] to get the total gain, including amplification via electronics (description of the electronics used in section 2.4.1).

To ensure that mostly SPE events are detected and that events take place within the QDC's integration window, LEDs send photons to each PMT to be measured with such a low intensity, that, on average, only every 10th pulse or less a single photon is detected. Then, shortly after the signal triggering the LEDs has been sent, the QDC is triggered with such a delay, that events correlating with LED pulses are entirely inside the integration window. The window width is big enough to contain a complete pulse as well as possible late pulses, but not too big, avoiding integrating over more than one main pulse or over afterpulses.

If no problems were encountered during measurement and the intensity was low enough, two peaks should be visible in the resulting charge histogram (figure 3.1, left). One of them is the SPE peak, its mean representing the mean charge being caused by measuring a single photon. The other one is the so called pedestal, resulting from the QDC integrating over the baseline with no pulse present. The latter happens if the respective LED is triggered without a photon being detected afterwards. Because the signal baseline is not at 0 V, integration over it yields a nonzero charge value, which has to be subtracted from the values gained for each pulse to correct them. For higher illumination intensities, indications of further peaks are visible in the spectra, which result from two PE events, three PE events etc. (figure 3.1, right).

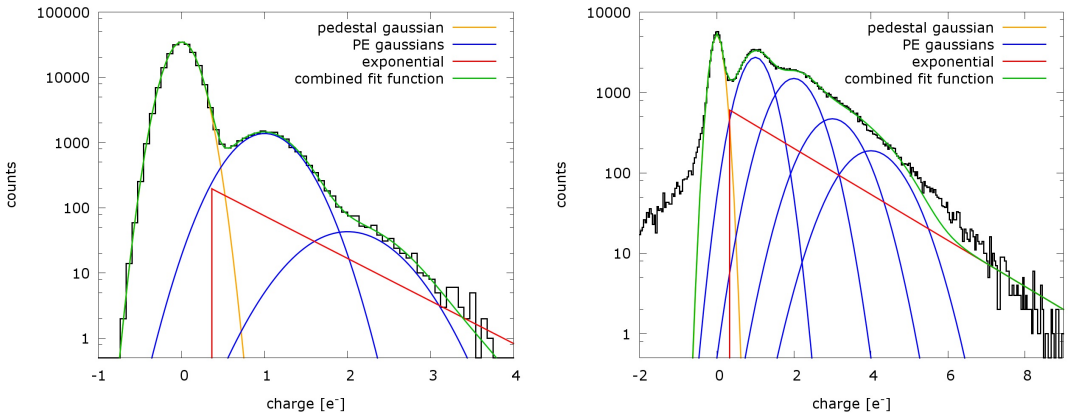

Figure 3.1.: QDC spectra. (Left) Low illumination. (Right) Higher illumination.

Determining the mean values for each peak is done by fitting the following functions

to the charge histogram, all parameters also being fit parameters [Kae]

$$f_1(x) = A_0 \exp\left[\frac{-(x-\mu_0)}{2{\sigma_0}^2}\right], \tag{3.1}$$

$$f_2(x) = \sum_{i=1}^{4} A_i \exp\left[\frac{-(x-i(\mu_1-\mu_0)+\mu_0)}{2i{\sigma_1}^2}\right] + B\exp(-x\tau), \tag{3.2}$$

with f_1 being fitted to the pedestal peak and f_2 to the SPE peak. Besides Gaussians in both functions, an additional, exponential part is included in the second one for phenomenological reasons, i.e. making the fit better. Usually, the exponential's amplitude is small, so that it does not introduce a bias in data. f_2 contains multiple Gaussians to account for the SPE peak as well as all peaks up to the 4 PE peak. This is necessary, as the amount of photoelectrons a PMT receives in the cooling setup can not be as well adjusted as in the room temperature setup, because the former only has 3 LEDs to illuminate all PMTs, while the latter has one individual LED for each PMT. Thus, usually 2 Gaussians are sufficient for fitting to data taken in the room temperature setup.

Gaussians belonging to events with more than 1 PE are set to be at a certain distance to the SPE peak, as an i PE peak should have an i-times larger distance to the baseline compared to the SPE peak. Also, because the amount of electrons a single photoelectron creates at the first dynodes can be assumed to follow a Poisson distribution, the standard deviation of the ith Gaussian is set to be $\sqrt{i}$ times the standard deviation of the first one. After fitting, the respective PMT's gain g is determined as follows, with μ_0 being the pedestal's mean value and μ_1 being the SPE mean value

$$g = \frac{\mu_1 - \mu_0}{10\ e}, \tag{3.3}$$

with the division by 10 resulting from the fact that a PMT's signal is amplified by this factor before being sent to the QDC, so it has to be accounted for to calculate the real gain.

The amount of electrons emitted from a dynode depends on the energy an incoming electron has before hitting it, which in turn depends on a PMT's voltage. As it can be assumed that the total number of electrons knocked out of one dynode is proportional to the applied voltage, one can argue that the gain is related to the latter in form of a power law, because each dynode multiplies the number of electrons coming in from

the dynode respective photocathode before it

$$g(U) = g_{wish} \left(\frac{U}{U_0} \right)^{\alpha}. \tag{3.4}$$

For practical reasons, this kind of function, with U_0 and α as free parameters, has been chosen, as it allows to to specify a certain gain g_{wish}, resulting in U_0 being the voltage required to reach that gain. For the experiment outlined here, $g_{wish} = 3 \times 10^6$ has been chosen.

To determine U_0, SPE charge histograms were taken for several different voltages between 1320 V and 1730 V to calculate the respective gain. The resulting gain-voltage diagram was then used to fit the function in equation (3.4) onto it. Additionally, the SPE peak's relative resolution R, which is defined as the peak's standard deviation divided by its mean value after subtracting the baseline

$$R := \frac{\sigma_1}{\mu_1 - \mu_0}, \tag{3.5}$$

as well as the so called "peak-to-valley ratio" (P/V), which is the SPE peak's height divided by the height of the valley between baseline peak and SPE peak, are calculated for some PMTs at room temperature and different voltages. Both parameters give insight about how well the charge of a single photoelectron can be resolved and how well the SPE peak can be differentiated from the baseline peak. As no appropriate algorithms were available, P/V has been determined manually, with errors resulting from reading the spectra assumed to be negligible compared to statistical errors. For the latter, it was assumed that the number of counts in a bin follows a Poisson distribution.

3.1.2. Results: Gain values at different temperatures and single photoelectron resolution parameters

Measurements at room temperature as well as $\approx -108\,^{\circ}\mathrm{C}$ have shown, that the aforementioned fit functions describe the data taken well within the relevant intervals. Figure 3.2 illustrates the voltage dependence of the gain.

Results at room temperature (table A.1 and table 3.3, left) furthermore show α to be generally very close to 8. The reason for this behavior, however, is unclear. For the

same reasons given for assuming a power law (section 3.1.1), a first guess would involve 8 being the number of the measured PMT's dynodes. Because the R11410 series has 12 dynodes, this is not the case.

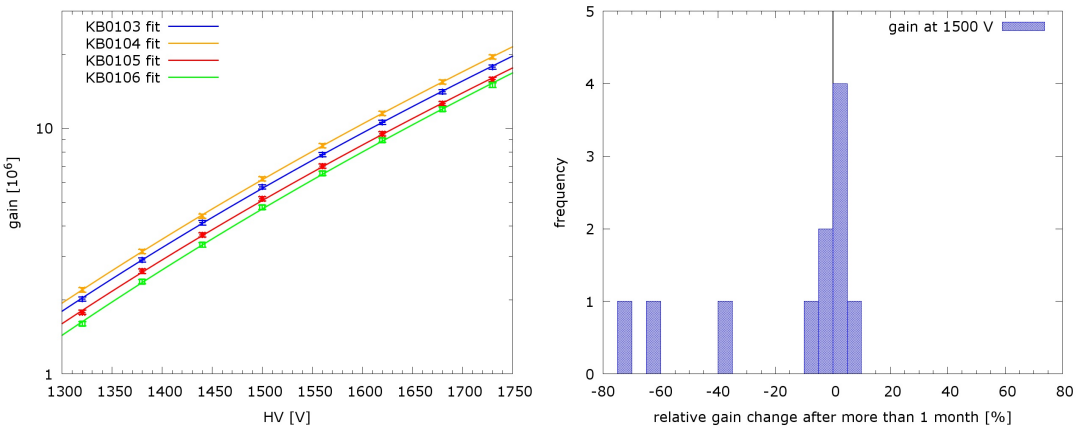

Figure 3.2.: Gain analysis at room temperature. (Left) Gain fits for 4 R11410-21 PMTs. (Right) Gain stability analysis.

For some PMTs, gain data from several test runs was available. With the exception of three outliers, relative changes of the gain at 1500 V between two measurements generally scatter around 0 % (figure 3.2, right), which is a sign that the gain can be assumed to be stable. Two of the three outliers were measured in exactly the same room temperature setup slot, where they have shown a much lower gain than they had during a past measurement. This slot has to be tested in the future for possible bias sources.

As for the SPE peak's relative resolution measured for 5 R11410-21 PMTs (equation (3.5)), one can see that it improves steadily up to 1500 V (figure 3.3, left). At higher voltages, it stays roughly the same at around (28.7 ± 0.8) %. P/V shows a similar behaviour, staying at about 4.70 ± 0.28 (figure 3.3, right). Both means were calculated by averaging over the respective values at the three highest voltages for each PMT. Consequently, it is necessary to apply at least a voltage of around 1500 V to the PMTs to obtain the maximum possible charge resolution.

When comparing room temperature HV-scan results with those at $\approx -108\,^{\circ}\mathrm{C}$ (table A.2 and table 3.3, right) for 10 PMTs, a slight increase in gain at lower temperatures has been observed, visible in comparison (figure 3.4, left). A histogram depicting the frequency of the certain relative change in gain between both temperatures at 1500 V

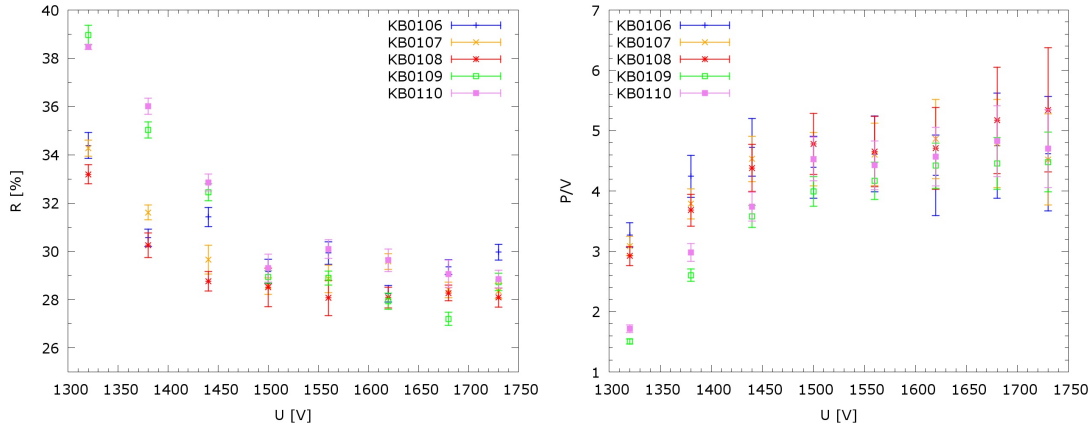

Figure 3.3.: Resolution parameters vs voltage. (Left) SPE resolution versus applied voltage. (Right) Peak-to-valley ratio versus applied voltage.

also hints at higher gain at lower temperature (figure 3.4, right). However, one has to account for possible QDC calibration errors, which could result in some QDC channels measuring a systematically different charge, as the PMTs were not connected to the same channels for both measurements. Differences in cabling length could also play a role, as the cables leading to the room-temperature setup have different lengths and thus a different resistance than those leading to the cooling setup. This would result in different signal heights and, consequently, different charges being measured. Concluding from these observations, further tests have to be made to make a definite statement on the gain change.

vers.	#	$\overline{U_0}$ [V] (≈23 °C)	$\overline{\alpha}$ (≈23 °C)	vers.	#	$\overline{U_0}$ [V] (≈−108 °C)	$\overline{\alpha}$ (≈−108 °C)
MOD	2	1380 ± 30	8.09 ± 0.06	MOD	2	1310 ± 90	8.30 ± 0.07
10	4	1390 ± 50	7.97 ± 0.08	10	2	1390 ± 60	8.09 ± 0.06
21	21	1460 ± 60	8.01 ± 0.09	21	6	1480 ± 70	8.35 ± 0.18

Table 3.3.: Gain results summary - Mean values and their standard deviations given as errors. # describes the number of PMTs measured.

Eventually, it is also necessary to compare the measured values with those given by Hamamatsu. As it can be seen in figure 3.5 (left), there is a linear relation between both, supported by the value of the Pearson correlation coefficient ($r = 0.97$). A histogram depicting relative gain changes compared to the respective Hamamatsu value (figure 3.5, right) reveals, that a systematically slightly higher gain (around 3 % on

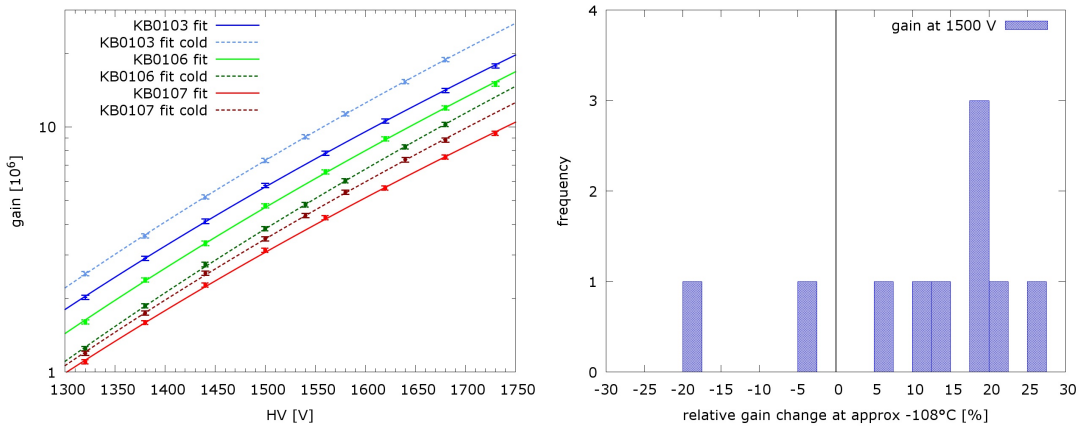

Figure 3.4.: Comparisons between room temp. and $\approx -108\,°C$. (Left) Gain fit comparison. (Right) Relative gain change.

average) has been measured. Otherwise, the measured values are in agreement with those from Hamamatsu. The typical value of 5×10^6 at 1500 V given in section 1.3.1, however, is not reached by the majority of the PMTs delivered so far.

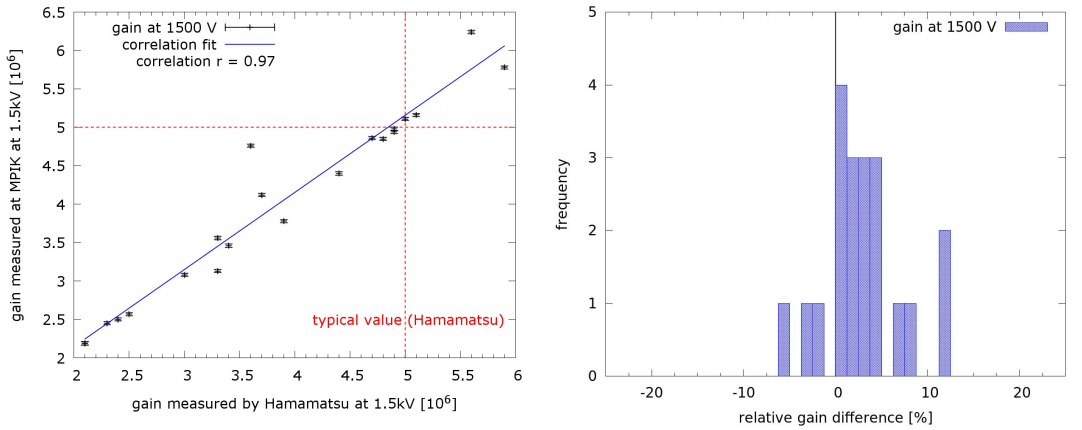

Figure 3.5.: Comparison with Hamamatsu specifications. (Left) Specification vs measured value. (Right) Relative gain difference compared to specification.

In conclusion, it can be said that the PMTs measured seem to have a stable gain, while their gain values furthermore are in agreement with those specified by the producer. Still, the reasons for measuring systematically higher gains than those specified by Hamamatsu as well as those for a seeming temperature dependence are unknown and currently under investigation.

3.2. Dark count rate

The dark count rate is the rate, at which electrons spontaneously released at the photocathode and dynodes (mostly caused by thermal emission) result in a measureable pulse indistinguishable from real ones. Keeping this rate low is vital to avoid random coincidences, which pose a hindrance when trying to detect very rare events, like those postulated for WIMP interaction with matter.

3.2.1. Measurement method and data analysis

Measuring a PMT's dark count rate is simply a matter of counting the number of pulses within a certain time interval without light being present. Using the scaler to count the number of pulses during a certain time interval, one is able to determine it by dividing this number by the length of the interval. This requires the dark count rate to be stable during measurement.

Because the PMTs see much light while inserting them into a setup, space charge accumulates at the photocathode, produced by ambient photons. When applying voltage to a PMT in this state, the charge is accelerated towards the first dynode, resulting in many more pulses occurring than normally via thermal emission and other sources. Thus, one has to wait for a PMT to “calm down” before measuring its dark rate. The waiting time depends on the amount of ambient light the PMTs have received. Four of the PMTs shown in figure 3.6 have seen much light, and it took roughly 33 h after mounting for their dark rate to be 10 % above the final value for each of them. Two of them (KB0115 and KB0116) have seen less light, and consequently, they only needed 18 h to reach the same deviation. Generally, a waiting time of about 1.5 days has been chosen in order to guarantee, that dark count rates are at their final value.

Also, the relative threshold above which the discriminator emits a pulse should be the same for all measurements and PMTs in order to make comparisons between them. To achieve this, the discriminator has been calibrated in such a way, that a signal is sent if the incoming pulse height is larger than approx. $\frac{1}{4}$ of an SPE pulse's height at a gain of $g = 3 \times 10^6$, requiring that each PMT has its respective U_0 applied to. The threshold needs to be at least approximately the same for each PMT channel, so that there are no differences in the kind of pulses which are taken into account.

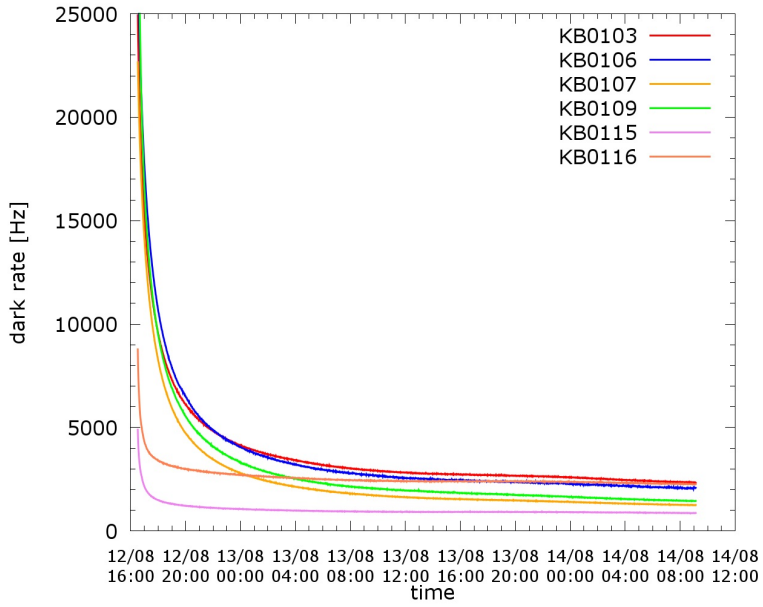

Figure 3.6.: Evolution of dark count rate, beginning 1 h after installation into setup.

Furthermore, each PMT's temperature has to be kept stable enough for them to be in thermal equilibrium with their environment. In case of the Faraday cage array, it is trivial, as it is at room temperature (20 ℃ - 25 ℃ mean as outlined in section 2.1) in a temperature-controlled room, resulting in minimal changes only. But when using the cooling setup, great care has to be taken to keep temperature stable enough for an at least prolonged amount of time. Because of the setup's good thermal isolation causing only a very slow change of temperature during the warm up phase after a cooldown, it allows a continuous measurement of the dark rate while mapping it to a corresponding temperature. This is because the PMT can be assumed in good approximation to be at the same temperature the respective sensors measure.

3.2.2. Results: Temperature dependence of the dark count rate

Plots in figure 3.7 of the dark count rate evolution at room temperature as well as at approximately liquid xenon temperature show stable values. Sometimes, singular peaks were visible in the data, caused by electronic noise (for instance raising/lowering the laboratory's shutters, neighboring experiments, etc.). Thus, those peaks either had to be removed, or intervals not containing such peaks had to be chosen for determining

the mean dark rate over a certain period of time.

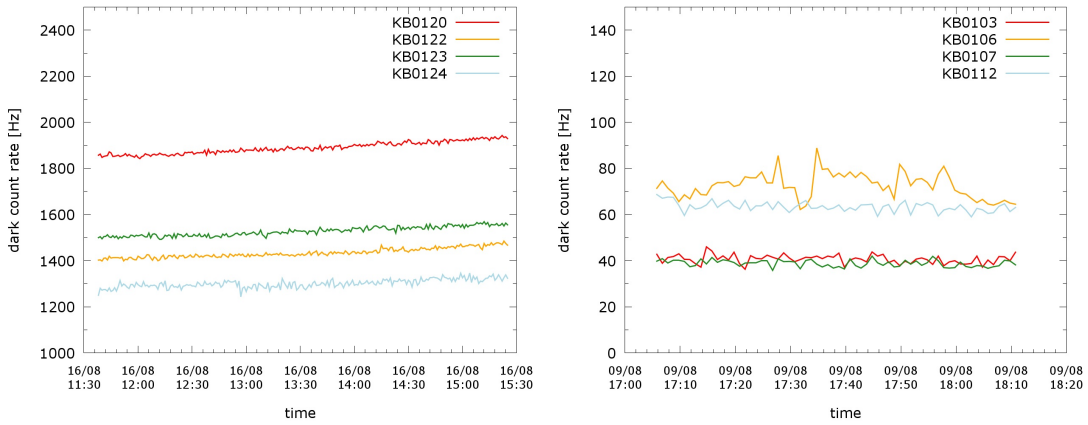

Figure 3.7.: Dark rate evolution over time. The slight drift to higher rates in the left plot resulted from an increase in room temperature. (Left) At $\approx$ 23 °C. (Right) At $\lesssim -100$ °C.

Averaging the dark count rate over a as large as possible time interval nets an average value of 1740 Hz with a standard deviation of $\sigma = 630$ Hz for the 20 PMTs of version R11410-21 measured (table A.3, figure 3.8, left). Although the spread is very large, none of the PMTs passed the typical value of 4000 Hz given by Hamamatsu (section 1.3.1), meaning that this particular characteristic is better than expected for room temperature, especially given the low threshold chosen. However, the threshold could not be set precisely and temperature was not closely monitored for measurements in the room temperature setup, so systematic errors are to be expected. They are still being analyzed at the time of writing and could not be included.

Of higher importance are the dark count rates near liquid xenon temperature, i.e. conditions the PMTs will be operating at in XENON1T. As mainly thermal emission causes dark pulses, dark count rates decreased significantly when cooling down the respective PMTs. Rates sharply decreased until down to about −20 ℃ (figure 3.9), where a plateau was reached. This is because of other, temperature-independent sources (for ex. radiation and cosmic rays) becoming dominant, as the amount of thermally emitted electrons decreases. The data is consistent with measurements done by the University of California [Lun+12], which have shown that those events mostly contain more than 1 PE. This means, that threshold differences in the setup do not play a critical role here, as each channel is guaranteed to trigger at heights corresponding to 1 PE and above.

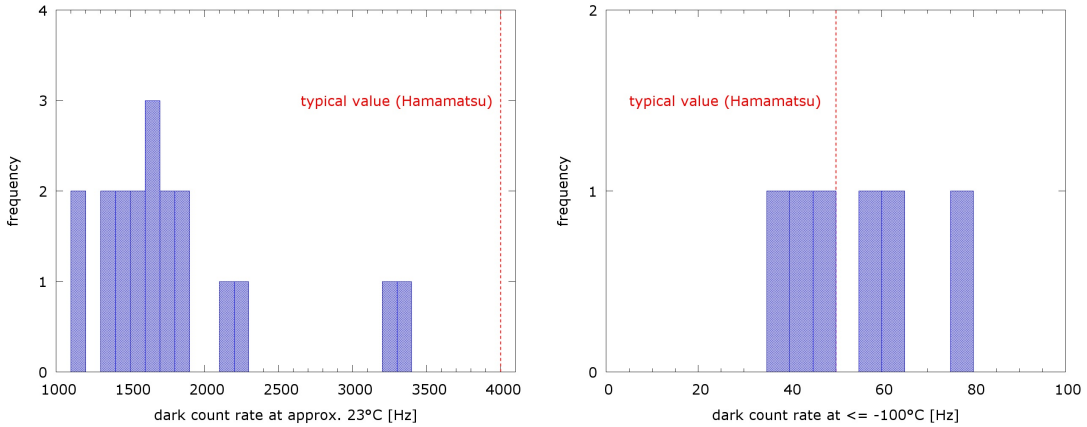

Figure 3.8.: Histograms showing the dark rate distribution among the measured PMTs. (Left) At $\approx 23\,^{\circ}\mathrm{C}$. (Right) At $\lesssim -100\,^{\circ}\mathrm{C}$.

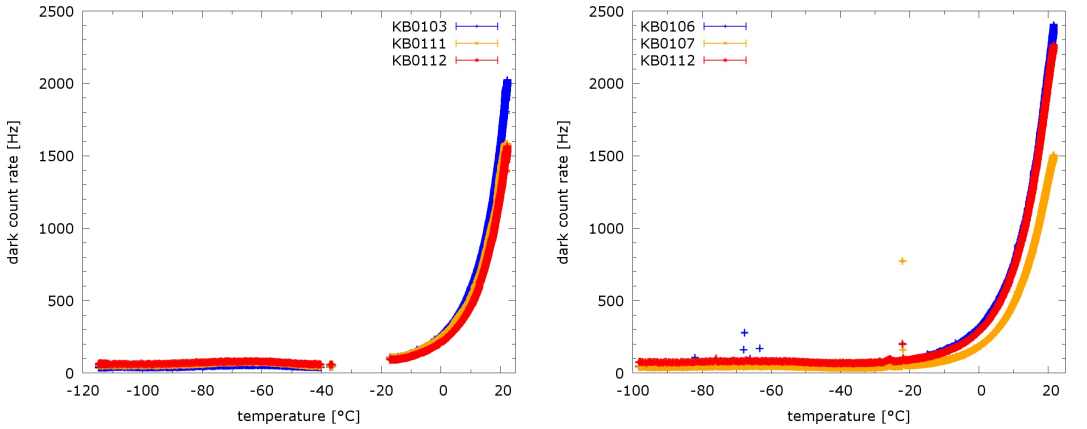

Figure 3.9.: T vs dark count rate. (Left) At U_0. (Right) At 1500 V.

A clarification is needed for the left plot in figure 3.9 showing a gap at a certian temperature range. This resulted from sudden noise problems occurring during measurement, because of which the respective data points had to be removed. There are also some outliers visible in the right plot, which were caused by electronic noise, such as the automatic shutter mechanism of the laboratory the setup used is located at.

Taking the average of the dark count rates measured for 6 version 21 PMTs during the stable phase of a cooldown with temperature fluctuations $\lesssim 1\,^{\circ}\mathrm{C}$ yields 54 Hz, with a standard deviation of 14 Hz (table A.3, figure 3.8, right). This is very close to the typical value Hamamatsu measured (50 Hz section 1.3.1). Though every PMT was at a temperature of $(-113 \pm 1)\,^{\circ}\mathrm{C}$, with the exception of 1 PMT at $(-99.8 \pm 0.8)\,^{\circ}\mathrm{C}$, the values are comparable to $-100\,^{\circ}\mathrm{C}$ due to being far within the aforementioned plateau region. The

temperature differences resulted from one PMT being mounted on a different structure and thus being at a different height than the other ones. Furthermore, because temperature has been closely monitored and threshold differences do not play a major role at such low temperatures, systematic errors should be negligible.

In summary, tests have confirmed the typical value given by Hamamatsu for a temperature of −100 ℃, which is the temperature which actually matters, as it is closest to XENON1T conditions. Also of importance is the fact, that the dark rates measured have shown themselves to be stable at both warm and cold temperatures. This enables the collaboration to reliably calculate rates for random coincidences, which is needed to estimate the time XENON1T can run with no WIMP event being found until those coincidences may pose a problem.

3.3. Transit time spread (TTS)

The transit time spread is the width of the distribution of the time it takes for a photoelectron to produce a pulse at the anode after being released from the photocathode. To attain a good coincidence resolution, which is necessary for XENON1T as it allows better event discrimination, the TTS needs to be kept low.

3.3.1. Measurement method and data analysis

Using the trigger board, two signals are sent periodically with a frequency of about 1028 Hz. One of them triggers the LEDs to emit photons at SPE intensity, the other one starts the TDC measurement. The latter is delayed in such a way, that the main pulses resulting from LED photons are within about 1.2 µs after it, as the TDC is only capable of measuring time differences up to this interval length (section 2.4.1).

In the resulting time histogram (figure 3.10), a main peak is visible, which corresponds to the average electron travel time inside the PMT. Because electrons are emitted at different positions within the PMT, they have different travel times, causing the peak to be asymmetric, as electrons released at the center of the photocathode take less time to travel to the first dynode than those released at the outer regions. To determine the full width at half maximum, which is equivalent to the TTS, an algorithm has been used [Kae].

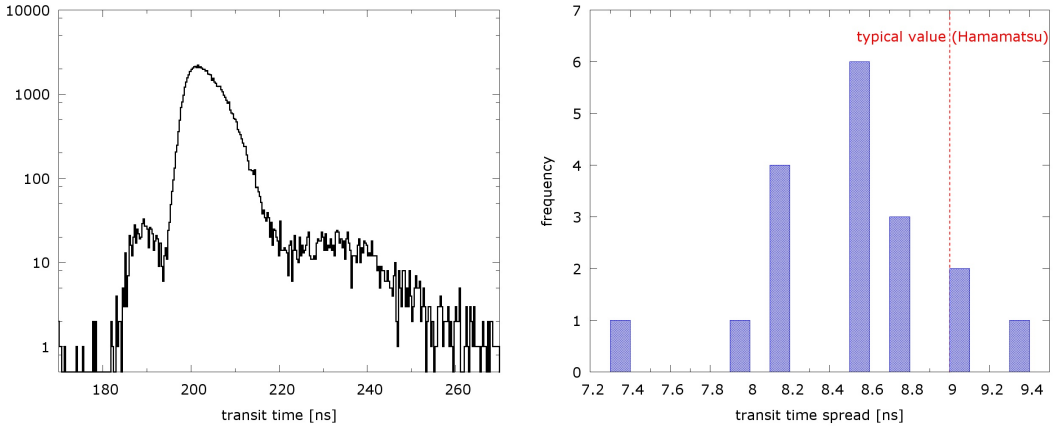

Figure 3.10.: (Left) TDC spectrum showing the transit time distribution. (Right) TTS comparison.

Left and right to the main peak are smaller, secondary peaks. The one occurring roughly 20 ns before the main pulse corresponds to early pulses, while the other one stretching to about 50 ns after the main pulse corresponds to late pulses. Both phenomena are explained in section 1.2.2.

3.3.2. Results: Transit time spread at room temperature

Tests made with 18 of the version-21 PMTs give an average value of 8.5 ns, with a standard deviation of $\sigma = 0.5\,\mathrm{ns}$ (table A.4, figure 3.10), which is close to the typical value of 9 ns given by Hamamatsu (section 1.3.1). Also, the average TTS is slightly below the sampling rate of 10 ns, which was used for XENON100 [Apr+12] and is also planned to be used for XENON1T. Consequently, it should only have a small impact on the detector's time resolution.

3.4. Afterpulses

Afterpulses are pulses caused by photoelectrons ionizing rest gas atoms/molecules within the PMT. These positively charged ions move towards the photocathode because of the electric field and release one or more electrons there. These electrons cause pulses indistinguishable from regular ones by themselves, meaning that the number of afterpulses needs to be kept low to avoid random coincidences with real detection signals.

3.4.1. Measurement method and data analysis

Measuring afterpulses is done in the following way: The TDC measurement starts at least 150 ns after a main pulse, so that no late pulses are within the measurement window of 1.2 µs. As only a single hit TDC was available for PMT testing, those pulses would otherwise completely suppress any pulses occurring after them. The LEDs illuminate the PMTs at MPE intensity (typically about 7 - 8 photoelectrons per pulse) to gain enough statistics within a reasonable amount of time.

In order to examine an interval at least as large as the one Hamamatsu used in their measurements (≈2 µs, section 1.3.1), several time histograms had to be combined. To achieve this, three TDC measurements have been done, with one starting at approximately 152 ns, and the other ones starting at about 1128 ns and 2020 ns after a main pulse respectively. The measured intervals overlap and result in a combined interval from 152 ns to 3133 ns.

Before combining the data, tough, the TDC's single hit limitation has to be accounted for, as events taking place at a later time within the time window are consequently measured with a lower probability than events taking place at an earlier time. The impact of this suppression is especially pronounced if there are many events at the beginning of the window. This effect can be partially corrected via statistical analysis. p_i represents the probability per main pulse of an event taking place which belongs to bin i of the time histogram, while p'_i is the measured probability. For an event to be measured, it requires that no events with a smaller time difference with respect to the TDC start signal, which belong to previous bins, have occurred

$$p'_i = p_i \prod_{k=1}^{i-1}(1 - p_k), \tag{3.6}$$

provided that bin probabilities are independent from each other and more than one afterpulse can occur in the given time interval.

Rearranging this equation to put p_i to the left side yields

$$\begin{aligned} p_i &= p'_i \left[\prod_{k=1}^{i-1}(1 - p_k)\right]^{-1}, \\ &= p'_i \alpha_i, \end{aligned} \tag{3.7}$$

with $p_1 = p'_1$, as there are no bins before the first one.

To determine p'_i from the measured data, the number of events measured in bin i, N'_i, is divided by the total number of measured main pulses N_{MP}, computable via the main pulse frequency f (at MPE intensity in very good approximation equal to the LED trigger frequency) and the time taken for the respective TDC measurement T

$$p'_i = \frac{N'_i}{N_{MP}}, \tag{3.8}$$

$$N_{MP} = f\,T. \tag{3.9}$$

This correction ansatz, however, neglects the detection efficiency of afterpulses. This effect can be assumed to be negligible, though, as the detection of afterpulses depends on a PMT's collection efficiency, which, according to Hamamatsu, is around 90 % [Lun+12] for most of the photocathode area of the PMTs tested. Thus, because of the high illumination intensity (7 - 8 photoelectrons per pulse on average), the probability for all created afterpulses to be not detected goes to zero. Dark pulses and afterpulses caused by afterpulses are also not taken into account. Dark pulses can be assumed to be negligible, if one takes the typical dark count rate into account (section 1.3.1). As an interval with a total length of ≈3 µs has been measured with a frequency of 1028 Hz for 500 s, one can estimate the total number of dark counts D_{tot} within the measured interval by

$$D_{tot} = 4000\,\mathrm{Hz} \cdot 3\mu\mathrm{s} \cdot 1028\,\mathrm{Hz} \cdot 500\,\mathrm{s} = 6168. \tag{3.10}$$

On average, 1.85×10^6 events have been measured in total, meaning that dark count events make up only about 0.33 % of them. Furthermore, because many PMTs have a much lower dark count rate (see section 3.2.2 and table A.3), dark pulses should not account for an error more significant than statistical fluctuations.

To be capable to compare the results with each other, they need to be normalized, as the afterpulse ratio also depends on the mean number of photons a main pulse encompasses. As it can be assumed that the probability for an afterpulse to be caused in a certain bin is, in good approximation, directly proportional to the number of photoelectrons the main pulse contains, the probability for a single photoelectron is:

$$p_i(1) = \frac{p_i(n)}{n}. \tag{3.11}$$

The corrected, normalized number of events for bin i, N_i, is then given by

$$N_i = p_i(1)N_{MP} = \frac{\alpha_i N'_i}{n}. \tag{3.12}$$

In order to calculate n, i.e. the average number of detected photoelectrons per main pulse, a charge histogram at exactly the same LED settings as for the afterpulse measurement has to be taken. Every second LED trigger pulse is suppressed to be able to integrate over the baseline, as at MPE intensity, almost every LED pulse results in photons being detected. Like with an SPE charge histogram, two peaks should be visible (figure 3.11): The baseline peak, and one similar to an SPE peak, but much larger and wider, the MPE peak. The MPE peak's width results in the peak being made up out of several overlapping Poisson peaks at charges corresponding to discrete photoelectron numbers, smeared (i.e. convoluted) with a Gaussian to represent the SPE resolution. Thus, a corresponding fit function containing 60 of those peaks has been used for fitting [Kae] within the area, where the MPE peak is located. As it can be seen in figure 3.11, the fit function describes the data well. The mean value μ of the underlying Poisson distribution is then converted into the mean number of incident photons via the respective PMT's gain factor, for which a value from a previously made gain measurement is used. The mean value of the baseline peak is also taken from a previous QDC measurement made for determining the gain.

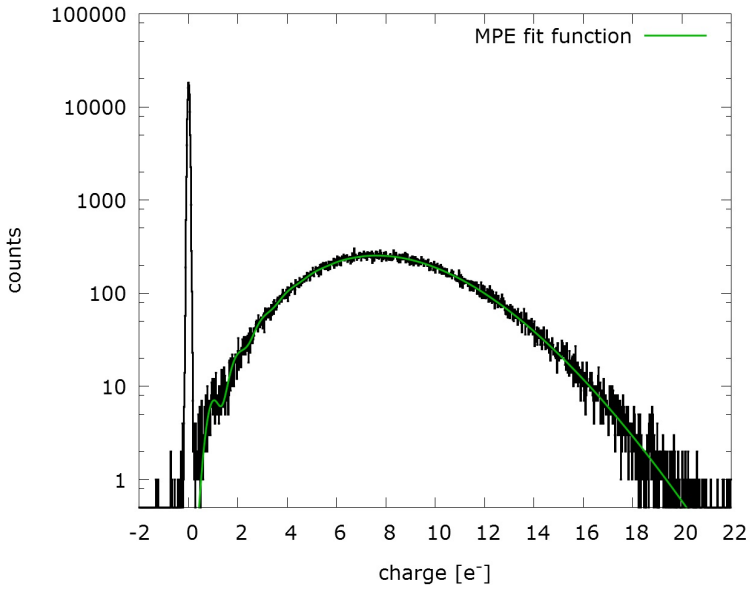

Figure 3.11.: MPE spectrum with corresponding fit function shown.

Finally, after applying the correction in equation (3.11) to each measurement separately and merging the data, the resulting ratio of afterpulses per main pulse per photoelectron within the combined time interval (consisting of M bins in total) is

$$r_{AP} = \sum_{i=1}^{M} \frac{N_i}{N_{MP}} = \sum_{i=1}^{M} p_i(1), \tag{3.13}$$

with the error, calculated via statistical error propagation, being:

$$\frac{\Delta p_i(n)}{p_i(n)} = \sqrt{\sum_{k=1}^{i-1} \left[\frac{\Delta p_k(n)}{1-p_k(n)}\right]^2 + \left(\frac{1}{\sqrt{N_i'}}\right)^2} \tag{3.14}$$

$$\begin{aligned} \Delta r_{AP} &= \frac{\sqrt{\sum_{i=1}^{M} \Delta p_i(n)^2}}{n} \\ &= \sqrt{\sum_{i=1}^{M} p_i(n)^2 \left(\sum_{k=1}^{i-1} \left[\frac{\Delta p_k(n)}{1-p_k(n)}\right]^2 + \left(\frac{1}{\sqrt{N_i'}}\right)^2\right)}\, n^{-1}. \end{aligned} \tag{3.15}$$

This assumes that the number of afterpulses measured in a certain bin is Poisson distributed. As the statistical error of n resulting from fitting is very small and no further statistical fluctuations have reliably been determined due to measurement uncertainties, it has been neglected. If no events were measured within a bin, its statistical error is $\Delta p_i(n) = 0$. Systematic errors could not be reliably determined within this thesis.

3.4.2. Results: Afterpulse probabilities and spectrum analysis

The results in table A.4 for 21 of the R11410-21 PMTs give an average afterpulse-to-main-pulse ratio per photoelectron of 3.6 % with a standard deviation of $\sigma = 1.5\,\%$. All ratios are below the maximum value of 10 % (section 1.3.1), even tough a larger interval than that used by Hamamatsu has been examined, which is expected to result in larger values than the typical one. However, after data evaluation, a correlation between the average number of photoelectrons per main pulse and the afterpulse-to-main-pulse ratio became apparent, as it can be seen in the plot on the right side of figure 3.12). A clear trend towards lower ratios at higher illuminations is visible, which is also indicated by the Pearson correlation coefficient ($r = -0.70$) . The cause of this is currently under investigation and not completely clear, so the afterpulse ratios given in table A.4 should be treated as preliminary. One assumption is, that PMTs

detecting too few photoelectrons have a non-negligible amount of events, where no photoelectrons have been measured. These lower the mean value obtained from analyzing the associated MPE spectrum, causing it to be smaller than the real average number of photoelectrons for pulses which are actually detected.

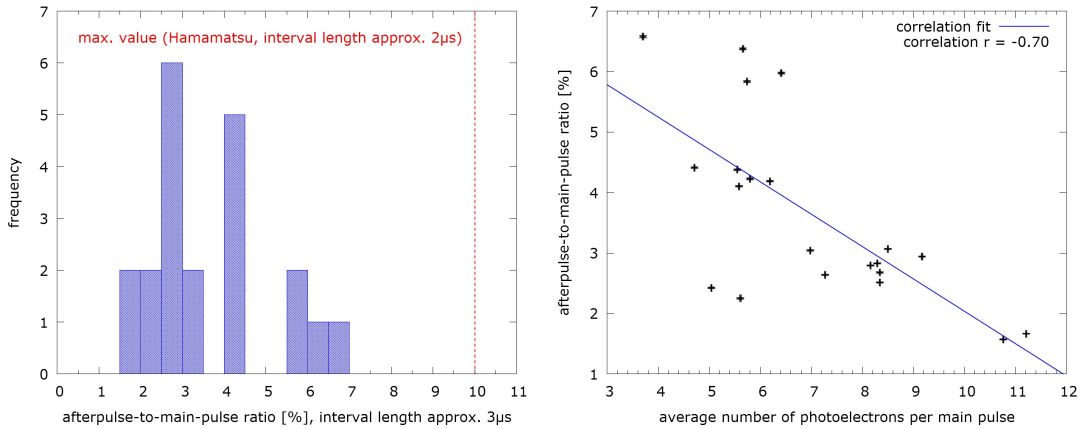

Figure 3.12.: (Left) Distribution of afterpulse-to-main-pulse ratio per photoelectron. (Right) Examination of correlation between afterpulse-to-main-pulse ratio and average number of photoelectrons per main pulse.

If one looks at the time histograms taken (figure 3.13), one can see several regularly appearing structures. One of those, here called “monotonically decreasing component”, stretches over the entire measured interval and has also seen in tests made by the University of Zürich [Bau+13]. What exactly causes this component is, as of yet, unclear.

The other ones are peaks appearing at fixed times in the interval. These have a known origin, namely ionized gas atoms/molecules, as it has been already mentioned in section 1.2.2. Using a similar plot published in [Lun+12], one is able to determine which kinds of gas cause those peaks to appear. In the afterpulse spectra of the measured PMTs, mainly peaks at about 1 µs, which correspond to CH_4^+, were visible, with sometimes an unknown peak at around 1.6 µs appearing. This peak roughly corresponds to the travel time Ar^+ or CO_2^+ would have, if one assumes ionization at the first dynode as well as a linear potential between it and the cathode [May]. Sometimes, also hints of an H_2^+ peak at roughly 0.5 µs could be made out. As the gases mentioned do not make up a significant amount of the atmosphere, they were probably used or appeared as a byproduct during the PMT production process.

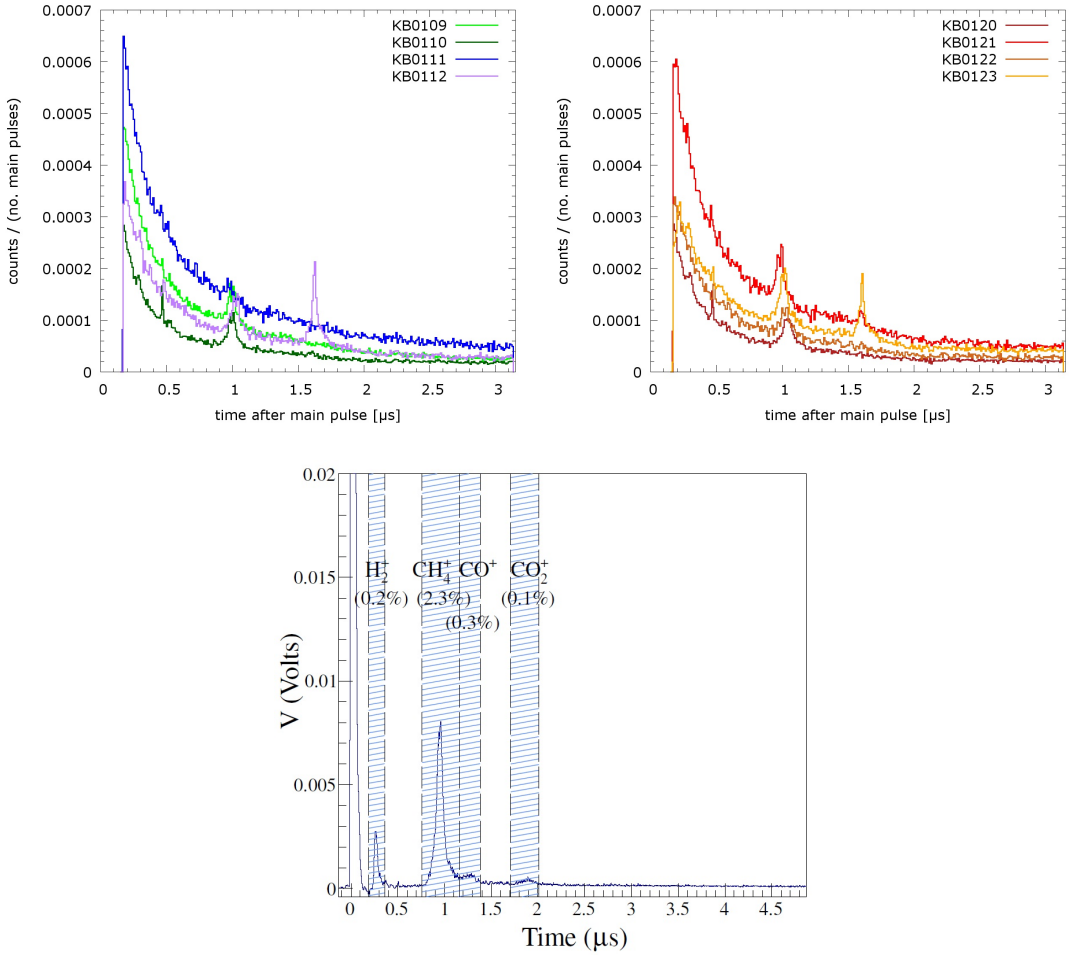

Figure 3.13.: Top: Normalized afterpulse plots of some R11410-21 PMTs. - Bottom: Afterpulse time spectrum from [Lun+12] below, where some peaks have been identified.

It is also important to look at if the afterpulse spectrum of a PMT changes after it has been cooled down, because new peaks appearing or peaks growing can be an indication of a leak letting air into the PMT. For the 7 PMTs (R11410-21) which were cooled down between 2 and 3 times, no additionally appearing peaks were visible, and their height relative to the monotonically decreasing component did not change suspiciously (figure 3.14). Differences in absolute values are very likely related to the aforementioned normalization problem, and because of this, only qualitative statements can be made.

At the end, despite normalization problems, it can be said that the PMTs are in accordance to the maximum afterpulse ratio Hamamatsu gives. This is reinforced by the fact, that there is a good probability that the bias caused by the normalization prob-

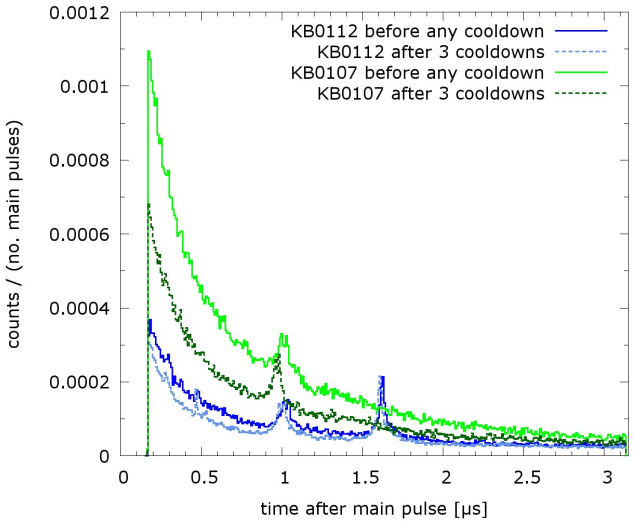

Figure 3.14.: Comparison of afterpulse spectra before any cooldown and after 3 cooldowns.

lem results in measured ratios which are larger than they actually are. Furthermore, Hamamatsu's maximum value is given for an interval of ≈2 µs (section 1.3.1), while the interval measured here is ≈3 µs long, so the latter is expected to take more afterpulses into account than the former. More importantly, no qualitative changes in the afterpulse spectra were made out for the cooled down PMTs, which would otherwise have hinted on air leaks being present.

4. Summary and outlook

In summary, several R11410-21 PMTs, which were designed for XENON1T in cooperation with Hamamatsu, were tested during the course of this bachelor thesis. The PMTs all have high quantum efficiencies at $\lambda = 175\,\mathrm{nm}$, which is the wavelength at which liquid xenon scintillates, as well as very low radioactivity levels. For each of them, gain, dark count rate, transit time spread and afterpulse-to-main-pulse ratio were measured at approximately 23 ℃. Gain and dark count rate were also measured at approximately −100 ℃ for 7 of the PMTs to evaluate them at a temperature near to the one they will operate at in XENON1T.

In terms of data analysis and acquisition, a range of algorithms and programs from previous PMT tests were present, at least for gain, dark count rate and transit time spread measurements. For afterpulse measurements, however, a correction algorithm had to be implemented to take systematic errors introduced by the limitations of the electronics, which have been used for testing, into account (section 3.4.1). Also, as the setup used for tests at low temperatures has been only recently constructed, its thermal sensors needed to be calibrated to provide reliable monitoring (section 2.4.2).

The results for each measured parameter were as follows:

- Gain measurements gave stable values close to Hamamatsu specifications.. For the relative SPE resolution as well as the peak-to-valley ratio, $R = (28.7 \pm 0.8)\,\%$ respectively $P/V = 4.70 \pm 0.28$ has been measured, with both of them being a limit the PMTs reach when applying voltages above 1500 V to them (section 3.1.2).

- Examining the dark count rate confirmed the typical value of 50 Hz at $-100\,^{\circ}\mathrm{C}$, while also showing that rates were stable at both warm and cold temperatures. This allows reliable calculations of random coincidence rates (section 3.2.2).

- The transit time spreads measured are close to the typical value of 9 ns given for them (section 3.3.2).
- Afterpulse-to-main-pulse-ratios were all below the maximum allowed value of 10 %. Furthermore, qualitative analysis of the afterpulse spectra have shown no suspicious changes for the PMTs which have been cooled down (number of cooldowns: 2 - 3) (section 3.4.2).

During some tests, phenomena with, as of yet, not definetly known origin have been encountered. Investigations are currently conducted to determine their sources. Another task, which needs to be done, is to improve illumination control in the cooling setup in order to allow transit time spread and afterpulse measurements at low temperatures. Both setup improvement and investigation of unknown occurrences are important for tests of future PMT batches, as they improve data validity and allow for a wider range of tests.

Nonetheless, because Hamatsu's specifications could be confirmed and no PMT has shown erratic behavior, a positive outlook remains. As of now, there is nothing against usage of the R11410-21 series in the XENON1T experiment, which should prove to be very useful if the high quantum efficiencies and extremely low radioactivity levels can be maintained during production.

A. Diagrams and data tables

A.1. Diagrams

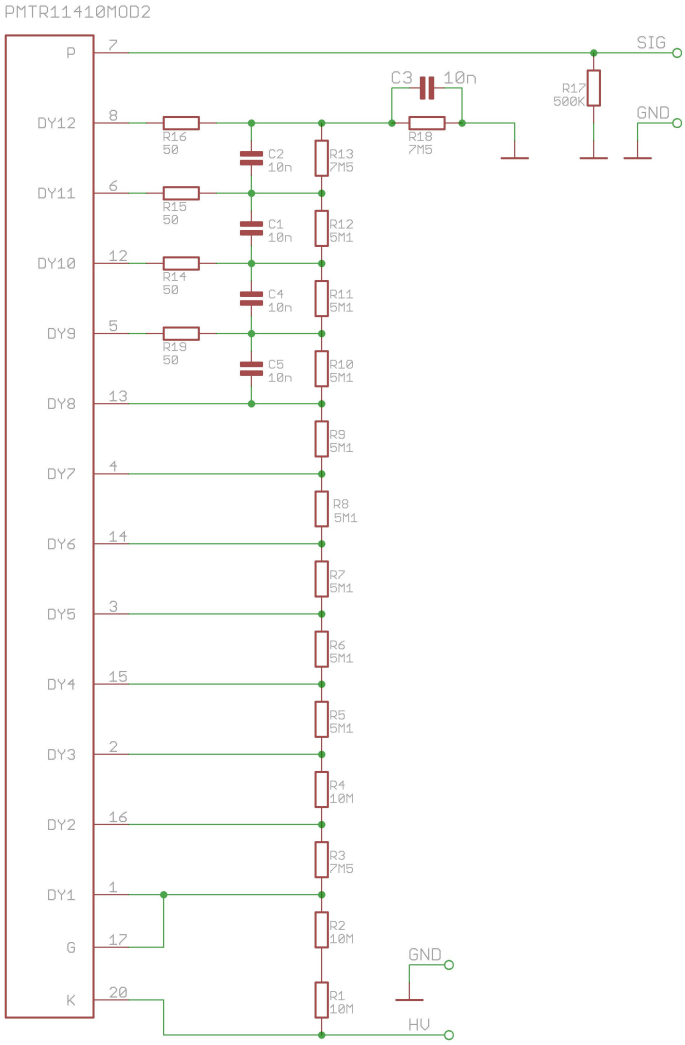

Figure A.1.: Circuit diagram of base

A.2. Detailed result tables for gain, dark count rate, TTS and afterpulse measurements

serial	vers.	α	U_0 [V]	g_{measured} (1.5 kV) [10^6]	$g_{\text{Hamamatsu}}$ (1.5 kV) [10^6]
ZK6008	MOD	8.09 ± 0.08	1360.0 ± 2.0	6.67 ± 0.03	-
ZK6010	MOD	8.09 ± 0.08	1408.1 ± 1.6	5.06 ± 0.03	-
KA0008	10	8.04 ± 0.08	1335.4 ± 2.1	7.62 ± 0.03	-
KA0009	10	7.94 ± 0.08	1361.2 ± 2.0	6.50 ± 0.03	-
KA0011	10	7.87 ± 0.07	1414.5 ± 1.6	4.82 ± 0.03	-
KA0017	10	8.04 ± 0.07	1437.8 ± 1.4	4.26 ± 0.03	-
KB0103	21	7.98 ± 0.08	1383.4 ± 1.8	5.78 ± 0.03	5.9
KB0104	21	8.08 ± 0.08	1371.6 ± 1.8	6.24 ± 0.03	5.6
KB0105	21	8.04 ± 0.07	1403.6 ± 1.5	5.16 ± 0.03	5.1
KB0106	21	8.25 ± 0.08	1420.2 ± 1.5	4.76 ± 0.03	3.6
KB0107	21	7.84 ± 0.08	1493.3 ± 1.4	3.13 ± 0.03	3.3
KB0108	21	7.89 ± 0.08	1497.3 ± 1.4	3.08 ± 0.03	3.0
KB0109	21	8.07 ± 0.07	1562.3 ± 1.4	2.19 ± 0.03	2.1
KB0110	21	7.99 ± 0.08	1563.3 ± 1.4	2.19 ± 0.03	2.1
KB0111	21	8.01 ± 0.08	1531.4 ± 1.4	2.57 ± 0.03	2.5
KB0112	21	8.04 ± 0.07	1541.3 ± 1.3	2.45 ± 0.03	2.3
KB0113	21	8.08 ± 0.09	1536.5 ± 1.4	2.50 ± 0.03	2.4
KB0115	21	8.00 ± 0.09	1413.2 ± 1.5	4.86 ± 0.03	4.7
KB0116	21	7.93 ± 0.09	1403.5 ± 1.7	5.11 ± 0.03	5.0
KB0117	21	8.01 ± 0.08	1441.5 ± 1.3	4.12 ± 0.03	3.7
KB0119	21	8.04 ± 0.09	1474.1 ± 1.3	3.46 ± 0.03	3.4
KB0120	21	7.89 ± 0.09	1469.2 ± 1.4	3.56 ± 0.03	3.3
KB0121	21	8.06 ± 0.08	1408.1 ± 1.5	4.98 ± 0.03	4.9
KB0122	21	7.97 ± 0.10	1460.2 ± 1.5	3.78 ± 0.03	3.9
KB0123	21	7.99 ± 0.09	1431.3 ± 1.5	4.40 ± 0.03	4.4
KB0124	21	7.98 ± 0.09	1413.2 ± 1.7	4.85 ± 0.03	4.8
KB0125	21	8.04 ± 0.09	1410.4 ± 1.5	4.94 ± 0.03	4.9

Table A.1.: Gain results at $\approx 23\,^{\circ}\mathrm{C}$. Only statistical fit errors could be included.

serial	vers.	α	U_0 [V]	g_{measured} (1.5 kV) [10^6]	measurement temperature [℃]
ZK6008	MOD	8.35 ± 0.09	1250.0 ± 2.7	6.67	-99.5 ± 0.5
ZK6010	MOD	8.25 ± 0.09	1378.0 ± 1.8	5.06	-99.5 ± 0.5
KA0009	10	8.06 ± 0.09	1342.0 ± 2.0	6.50	-99.5 ± 0.5
KA0017	10	8.12 ± 0.09	1425.3 ± 1.6	4.26	-99.5 ± 0.5
KB0103	21	8.13 ± 0.09	1340.7 ± 2.1	5.78	-112.6 ± 0.8
KB0106	21	8.58 ± 0.09	1456.3 ± 1.3	4.76	-112.6 ± 0.8
KB0107	21	8.28 ± 0.09	1470.9 ± 1.3	3.13	-112.6 ± 0.8
KB0110	21	8.32 ± 0.08	1562.4 ± 1.5	2.19	-99.5 ± 0.5
KB0111	21	8.20 ± 0.09	1509.0 ± 1.3	2.57	-112.6 ± 0.8
KB0112	21	8.17 ± 0.10	1508.4 ± 1.3	2.45	-112.6 ± 0.8

Table A.2.: Gain results at cold temperatures. Only statistical fit errors could be included (except for temperatures). Temperatures averaged over measurement time ($\approx 55\,\text{min}$) with standard deviation as error.

serial	vers.	dark count rate [Hz] ($\approx 23\,^{\circ}\mathrm{C}$)	dark count rate [Hz] (cold)	cold measurement temp. [℃]
KB0103	21	2281.4 ± 1.5	40.86 ± 0.19	-113 ± 1
KB0104	21	1661 ± 5	-	-
KB0105	21	1455.0 ± 1.1	-	-
KB0106	21	1828.1 ± 1.4	75.7 ± 0.9	-113 ± 1
KB0107	21	1100.5 ± 1.0	38.80 ± 0.15	-113 ± 1
KB0108	21	1644.4 ± 1.1	-	-
KB0109	21	1565.5 ± 1.7	-	-
KB0110	21	1148.9 ± 1.0	49.40 ± 0.21	-99.8 ± 0.8
KB0111	21	3225 ± 14	55.64 ± 0.26	-113 ± 1
KB0112	21	1734.8 ± 1.5	62.94 ± 0.23	-113 ± 1
KB0113	21	3356.0 ± 1.1	-	-
KB0115	21	809.2 ± 0.4	-	-
KB0116	21	2130.2 ± 0.8	-	-
KB0117	21	1700.3 ± 0.6	-	-
KB0120	21	1889.5 ± 1.7	-	-
KB0121	21	1640.5 ± 2.2	-	-
KB0122	21	1434.0 ± 1.3	-	-
KB0123	21	1527.4 ± 1.3	-	-
KB0124	21	1301.3 ± 1.2	-	-
KB0125	21	1352.4 ± 1.6	-	-

Table A.3.: Dark count rate results. Measurement interval length for KB0103-KB0112 21 min (warm) and 98 min (cold), for KB0113-KB0119 120 min and for KB0120-KB0125 228 min. The bigger the statistical error of the average dark count rate, the more it varied during measurement. Temperatures averaged over respective measurement time with standard deviation as error.

serial	vers.	transit time spread [ns]	afterpulse-per-main-pulse ratio [%]	mean number of photoelectrons per main pulse
KB0103	21	7.91 ± 0.02	2.677 ± 0.008	8.34 ± 0.01
KB0104	21	-	2.997 ± 0.024	3.040 ± 0.009
KB0105	21	-	5.85 ± 0.03	5.834 ± 0.013
KB0106	21	8.50 ± 0.02	4.410 ± 0.013	4.71 ± 0.01
KB0107	21	8.20 ± 0.02	6.557 ± 0.018	3.70 ± 0.01
KB0108	21	-	4.397 ± 0.029	4.378 ± 0.012
KB0109	21	8.79 ± 0.03	2.790 ± 0.008	8.16 ± 0.01
KB0110	21	8.20 ± 0.03	1.570 ± 0.005	10.76 ± 0.01
KB0111	21	8.50 ± 0.01	4.225 ± 0.012	5.80 ± 0.01
KB0112	21	8.50 ± 0.02	2.511 ± 0.009	8.34 ± 0.01
KB0113	21	8.20 ± 0.04	4.102 ± 0.012	5.58 ± 0.01
KB0115	21	8.79 ± 0.01	2.421 ± 0.010	5.04 ± 0.01
KB0116	21	8.50 ± 0.02	3.066 ± 0.008	8.50 ± 0.01
KB0117	21	9.38 ± 0.02	2.637 ± 0.008	7.27 ± 0.01
KB0119	21	8.50 ± 0.02	6.375 ± 0.014	5.66 ± 0.01
KB0120	21	9.08 ± 0.02	1.665 ± 0.005	11.21 ± 0.01
KB0121	21	8.20 ± 0.05	4.185 ± 0.011	6.19 ± 0.01
KB0122	21	7.32 ± 0.01	2.250 ± 0.009	5.61 ± 0.01
KB0123	21	8.50 ± 0.02	2.940 ± 0.008	9.17 ± 0.01
KB0124	21	9.08 ± 0.02	2.828 ± 0.008	8.29 ± 0.01
KB0125	21	8.79 ± 0.02	5.973 ± 0.013	6.41 ± 0.01

Table A.4.: Transit time spread results and afterpulse-per-main-pulse ratios for interval [152 ns - 3100 ns] after main pulse with respective mean number of photoelectrons per main pulse, both at $\approx 23\,^{\circ}\mathrm{C}$. Only statistical fit errors could be included for the transit time spread and the mean number of photoelectrons.

Sources

[Apr+11] E. Aprile et al. “Design and Performance of the XENON10 Dark Matter Experiment”. *Astroparticle Physics* 34 (2011). DOI: 10.1016/j.astropartphys.2011.01.006. arXiv:1001.2834 [astro-ph.IM].

[Apr+12] E. Aprile et al. “The XENON100 Dark Matter Experiment”. *Astroparticle Physics* 35 (2012). DOI: 10.1016/j.astropartphys.2012.01.003. arXiv:1107.2155 [astro-ph.IM].

[Apr12] Elena Aprile. “The XENON1T Dark Matter Search Experiment” (2012). arXiv:1206.6288 [astro-ph.IM].

[Bar] Peter Barrow. Private communication. University of Zürich, Zürich, Switzerland, 2013.

[Bau+11] C. Bauer et al. “Qualification Tests of 474 Photomultiplier Tubes for the Inner Detector of the Double Chooz Experiment”. *Jorunal of Instrumentation* 6 (2011). DOI: 10.1088/1748-0221/6/06/P06008. arXiv:1104.0758 [physics.ins-det].

[Bau+13] L. Baudis et al. “Performance of the Hamamatsu R11410 Photomultiplier Tube in cryogenic Xenon Environments”. *Jorunal of Instrumentation* 8 (2013). DOI: 10.1088/1748-0221/8/04/P04026. arXiv:1303.0226 [astro-ph.IM].

[Ber10] Gianfranco Bertone. “The moment of truth for WIMP Dark Matter”. *Nature* 468 (2010). DOI: 10.1038/nature09509. arXiv:1011.3532 [astro-ph.CO].

[Gre] Greisinger electronic GmbH. Germany. URL: http://www.greisinger.de/.

[Ham] Hamamatsu Photonics K.K. Japan. URL: http://www.hamamatsu.com/us/en/index.html.

[Ham07] Hamamatsu Photonics. *Photomultiplier Tubes - Basics and Applications*. 3a. Aug. 2007. URL: http://www.hamamatsu.com/resources/pdf/etd/PMT_handbook_v3aE.pdf.

[Has10] J. Haser. "Die Datennahmekette des Double Chooz Experiments und ihre Komponenten - Eigenschaften der Photomultiplier und der Frontend-Elektronik". German. Diploma thesis. Ruprecht-Karls-Universität Heidelberg, July 1, 2010. URL: http://www.mpi-hd.mpg.de/lin/allpublications.de.html.

[Kae] Florian Kaether. Private communication. MPI für Kernphysik, Heidelberg, Germany, 2013.

[LHC] Large Hadron Collider. CERN, Geneva, Switzerland. URL: http://home.web.cern.ch/about/accelerators/large-hadron-collider.

[LNGS] Laboratori Nazionali del Gran Sasso. Italy. URL: http://www.lngs.infn.it/.

[Luc09] S. Lucht. "Kalibrierung der Sensitivität und Verstärkung der Photomultiplier für das Double-Chooz-Experiment". German. Diploma thesis. Rheinisch-Westfälische Technische Hochschule Aachen, Apr. 27, 2009. URL: http://www.physik.rwth-aachen.de/institute/institut-iiib/forschung/double-chooz/veroeffentlichungen/.

[Lun+12] K. Lung et al. "Characterization of the Hamamatsu R11410-10 3-Inch Photomultiplier Tube for Liquid Xenon Dark Matter Direct Detection Experiments". *Nuclear Instruments and Methods* A696 (2012). DOI: 10.1016/j.nima.2012.08.052. arXiv:1202.2628 [physics.ins-det].

[Mar] Teresa Marrodán Undagoitia. Private communication. MPI für Kernphysik, Heidelberg, Germany, 2013.

[May] Daniel Mayani. Private communication. University of Zürich, Zürich, Switzerland, 2013.

[NIC] National Instruments Corporation. Germany. URL: http://www.ni.com/labview/d/.

[Sch08] P. Schneider. *Einführung in die extragalaktische Astronomie und Kosmologie*. 2008. ISBN: 978-3540258322.

[WuT] Wiesemann & Theis GmbH. Germany. URL: http://www.wut.de/.

[XEN] XENON1T collaboration. Private communication. 2013.

Declaration

I hereby assert that I have written this thesis by myself and that no other than the sources and aids referred to have been used.

Heidelberg, August 26, 2013 Dominick Cichon